Modelling Strong Discontinuities in Solid Mechanics Via Strain Softening Constitutive Equations

J. Oliver

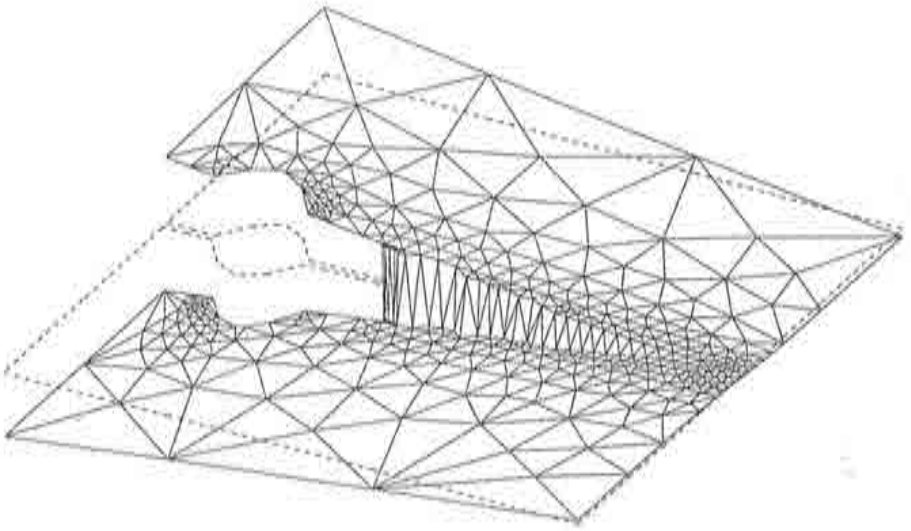

Monograph CIMNE Nº 28, May 1995

Modelling Strong Discontinuities in Solid Mechanics Via Strain Softening Constitutive Equations

Fundamentals
and
Numerical Simulation

J. Oliver
E.T.S. d'Enginyers de Camins, Canals i Ports
Technical University of Catalonia

Monograph CIMNE Nº 28, May 1995

To Prof. Juan C. Simo
"In memoriam"

Internacional Center for Numerical Methods in Engineering
Gran Capitán s/n, 08034 Barcelona, España

Diseño de la cubierta: Jordi Pallí

Primera Edición, Mayo 1995

Edita:
Centro Internacional de Métodos Numéricos en Ingeniería
Edificio C1, Campus Norte UPC
Gran Capitán, s/n
08034 Barcelona, España

ISBN: 84-87867-54-5
Deposito Legal: B-25750-95

PART I:

FUNDAMENTALS

SUMMARY

This part addresses some fundamental aspects about the use of standard constitutive equations to model strong discontinuities (cracks, shear bands, slip lines etc.) in solid mechanics analyzes. The so called strong discontinuity analysis is introduced as a basic tool to derive a general framework, in which different families of constitutive equations can be inscribed, then allowing to extract relevant aspects for the intended analysis. In particular, a link between continuum and discrete approaches to the strain localization phenomena is obtained. Applications to standard continuum damage and elasto-plastic constitutive equations are presented. Relevant aspects to be considered in the numerical simulation of the problem (tackled in Part II of the work) are also presented.

1. INTRODUCTION

Regular solid mechanics analyzes are generally conducted in the context of the *strict* Continuum Mechanics where continuity of the displacement field is postulated. However, in many engineering problems consideration of jumps in the displacement field is essential: cracks in rocks or concrete, slip lines in soils and shear bands in metals (when observed from a macroscopic point of view), have necessarily to be regarded when the aim of the analysis is to approach limit situations close to intensive damage or collapse. From now on we will understand by *strong discontinuities* these jumps in the displacement field appearing at a certain time, in general unknown before the analysis, of the loading history and developing across paths of the solid which are material (fixed) surfaces. They have to be distinguished from *weak discontinuities* that correspond to jumps in the strain field (the displacement remaining continuous) which develop along moving surfaces[7].

The presently available methodologies for the numerical simulation of strong discontinuities could be classified in two large families: discrete and continuum approaches.

Discrete approaches[3–6] are close to classical non linear Fracture Mechanics and consider specific traction vector vs. jump constitutive equations to characterize the cohesive behaviour at the discontinuity interface, whereas for the continuous part of the body regular stress-strain constitutive equations are used. In addition, appropriate criteria for the determination of the initiation and propagation of the discontinuity have to be considered.

On the contrary, in *continuum* approaches the complete solid is regarded from a Continuum Mechanics environment: the concept of strain is defined not only in the continuous part of the body, but also at the discontinuous interface and, therefore, standard stress-strain constitutive equations can be considered everywhere. Then, the discontinuity is modelled via two basic ingredients: a) an implicit (sometimes not recognized) regularization of the discontinuous displacement field which is approximated by means of high displacement gradients (strain localization) in a band whose width is characterized by the so called *characteristic length* which is taken as a material property[1] or as a numerical parameter [9], and b) special constitutive equations whose particular structure leads to the well posedness of the partial differential equations governing the problem and allowing the strain localization to appear. In the last years, much effort has been devoted to develop different approaches belonging to this family: the *smeared* crack methods using (regularized) local constitutive equations exhibiting strain softening[11,18], non local constitutive equations[14], Cosserat continuum, gradient plasticity[2], viscoplasticity [8] (or in general visco-regularized constitutive equations) could be mentioned as typical examples.

In this work the concept of *strong discontinuity analysis* already introduced in previous works[15,12,16,10], is used to bridge from continuum to discrete approaches. The aim of the analysis is to identify, in a general framework independent of the numerical method of simulation, the key qualitative features that make the standard stress-strain constitutive equations consistent with the appearance of strong discontinuities. In particular the analysis provides a *discrete* (i.e., stress vs. displacement-jump) constitutive equation at the discontinuity path which is consistent with the chosen *continuum* (stress-strain) constitutive equation. At this point it is possible to chose for modelling purposes between:

- a *continuum framework*: by regularizing the discontinuous displacement field (in such a way that the strains are bounded everywhere) and then using standard stress-strain constitutive equations.

- a *discrete framework*: by using the derived set of discrete (stress vs. displacement-jump) constitutive equations to describe the cohesive behaviour of the discontinuity path.

In order to state the generality of the analysis, it is driven for two different families of constitutive equations: continuum damage and elasto-plasticity models. Then, it is shown that, in spite of the differences between these

constitutive equations, a common methodology of analysis can be applied in both cases which can be easily extended to other constitutive equations.

On the other hand a set of relevant points emerging from the strong discontinuity analysis can be directly used in the design of specific finite elements for capturing strong discontinuities, in such a way that many unsuitable features of classical approaches (mesh-size and mesh-alignment dependencies, intrinsic limitations on the element size etc...) can be automatically removed. This topic will be addressed in a second part of this work.

2. KINEMATICS: DISCONTINUOUS DISPLACEMENT FIELDS

Let us consider the reference configuration Ω of a body exhibiting strong discontinuities along a discontinuity path $\mathcal{S}$ which is a material surface (i.e. fixed at the reference configuration) with a unit normal vector $\mathbf{n}$ (see Fig. 1).

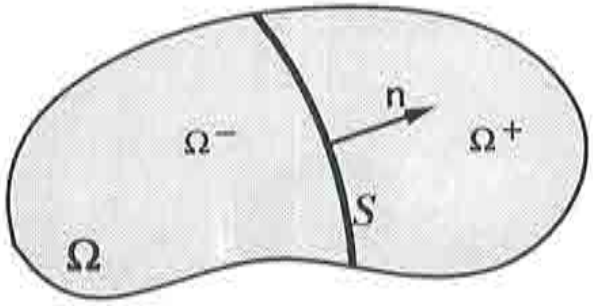

Figure 1. *Definition of the discontinuity path.*

For practical purposes we can assume that $\mathcal{S}$ splits the body into two parts ‡ Ω^+ and Ω^- in such a way that a Heaviside function $H_{\mathcal{S}}(\mathbf{x})$ ($\mathbf{x}$ being the material coordinates of the particles, $H_{\mathcal{S}}(\mathbf{x}) = 1\ \forall \mathbf{x} \in \Omega^+$ and $H_{\mathcal{S}}(\mathbf{x}) = 0\ \forall \mathbf{x} \in \Omega^-$) can be defined on Ω. The most general expression of a displacement field exhibiting strong discontinuities in $\mathcal{S}$ can be written as:

$$\mathbf{u}(\mathbf{x},\ t) = \bar{\mathbf{u}}(\mathbf{x},\ t) + H_{\mathcal{S}}\ (\mathbf{x})[\![\mathbf{u}]\!](\mathbf{x},\ t) \tag{2.1}$$

where t refers to time, $\bar{\mathbf{u}}(\mathbf{x},\ t)$ is the regular part of the displacement field and $[\![\mathbf{u}]\!](\mathbf{x},\ t)$ is a displacement jump function which is continuous everywhere in the body ‡‡. In Fig. 2 the displacement decomposition (2.3) is depicted for 1D cases.

From eq.(2.1) a jump $[\![\mathbf{u}]\!]_{\mathcal{S}}$ of the field $\mathbf{u}$ appears in $\mathcal{S}$ as:

$$[\![\mathbf{u}]\!](\mathbf{x},\ t)|_{\mathbf{x}\in\mathcal{S}} \ = \ [\![\mathbf{u}]\!]_{\mathcal{S}} \tag{2.2}$$

‡ strictly speaking $\mathcal{S}$ could be thought as the discontinuity path (not necessarily splitting the body) plus *any* extension splitting the body and allowing Ω^+ and Ω^- to be defined.

‡‡ the discontinuity of the resulting displacement field in eq.(2.1) is then achieved through the jump of the Heaviside function $H_{\mathcal{S}}$ across $\mathcal{S}$.

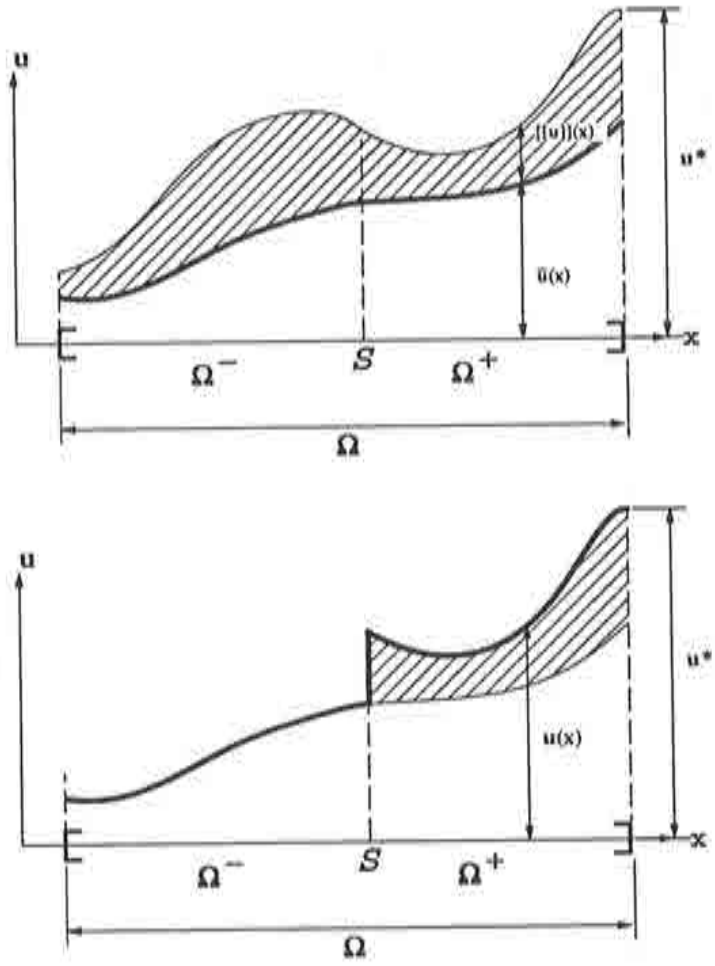

Figure 2. *Kinematic decomposition of the displacement field.*

The corresponding strain field can be obtained by computing the symmetric part of the gradient of the displacement field of eq.(2.1), this leading to:

$$\begin{aligned}\boldsymbol{\epsilon} = (\nabla \mathbf{u})^S &= \underbrace{(\nabla \bar{\mathbf{u}})^S + H_S\,(\nabla [\![\mathbf{u}]\!])^S}_{\bar{\boldsymbol{\epsilon}}} + \delta_S\,([\![\mathbf{u}]\!] \otimes \mathbf{n})^S \\ &= \bar{\boldsymbol{\epsilon}} + \delta_S\,([\![\mathbf{u}]\!] \otimes \mathbf{n})^S\end{aligned} \tag{2.3}$$

where superscript $(\cdot)^S$ means the symmetric part of $(\cdot)$ and δ_S is the Dirac's line delta-function along S, satisfying:

$$\int_\Omega \delta_S\ \varphi_0\ d\Omega = \int_S \varphi_0\ d\Gamma \qquad \forall\ \varphi_0 \in C_0^\infty\ (\Omega) \tag{2.4}$$

In eq.(2.3) the terms $(\nabla \bar{\mathbf{u}})^S$ and $H_S(\nabla [\![\mathbf{u}]\!])^S$ have been collected in the term $\bar{\boldsymbol{\epsilon}}$, that is, the regular part of the strain field exhibiting, at most, *bounded*

discontinuities. The unbounded character of the term $\delta_S([\![\mathbf{u}]\!] \otimes \mathbf{n})^S$ emerges from the gradient of the Heaviside function appearing in eq.(2.1).

3. STRONG DISCONTINUITY ANALYSIS

The concept of strong discontinuity analysis applies to any standard constitutive equation. The goal of the analysis is to extract the key qualitative features that make such a constitutive equation *consistent* with the appearance of strong discontinuities and , thus, with the unbounded strain fields (3.3). For this purpose the following set of requeriments is imposed on the stress field provided by the constitutive equation:

I) The stress field is *bounded* everywhere in the solid.

II) The *traction vector is continuous across* S at any time of the analysis.

III) At any point P of the discontinuity surface S the normal $\mathbf{n}$ is provided by the stress field at the *initation time* (the time where the discontinuity initiates at the considered point P).

Justification of condition I) comes from the nonphysical sense of unbounded stresses (even at the discontinuity path S, where the strains are unbounded according to eq.(2.3)). Condition II) emerges from the equilibrium conditions across the discontinuity path or, more formally, from the balance laws (see reference [16] for more details). Finally, condition III) stablishes the material surface character of S thus precluding any evolution of $\mathbf{n}$ beyond the initiation time.

In the next sections two different constitutive equations, belonging to the families of *continuum damage* and *plasticity* models are analyzed from the preceding point of view.

4. STRONG DISCONTINUITY ANALYSIS OF DAMAGE MODELS

4.1. An isotropic continuum damage model

Let us consider the family of constitutive equations defined by[11]:

$$\Psi = (1-d)\Psi_0 \qquad \Psi_0 = \frac{1}{2}\,\boldsymbol{\epsilon} : \mathbf{C} : \boldsymbol{\epsilon} \tag{4.1.1}$$

$$\boldsymbol{\sigma} = \frac{\partial \Psi}{\partial \boldsymbol{\epsilon}} = (1-d)\,\mathbf{C} : \boldsymbol{\epsilon} \tag{4.1.2}$$

where Ψ is the Helmholz's free energy, $\mathbf{C}$ the elastic constitutive tensor, $\boldsymbol{\sigma}$ the stress tensor and d the scalar damage variable ($0 \leq d \leq 1$). The value of the internal variable d is given by the corresponding damage condition and evolution laws. After some specialization[11] the damage variable evolution can be integrated in close form at time t giving:

$$\begin{aligned} d_t &= G(r_t) \\ r_t &= \max_{s\in(-\infty,t)} \{r_0, r_s^*\} \end{aligned} \tag{4.1.3}$$

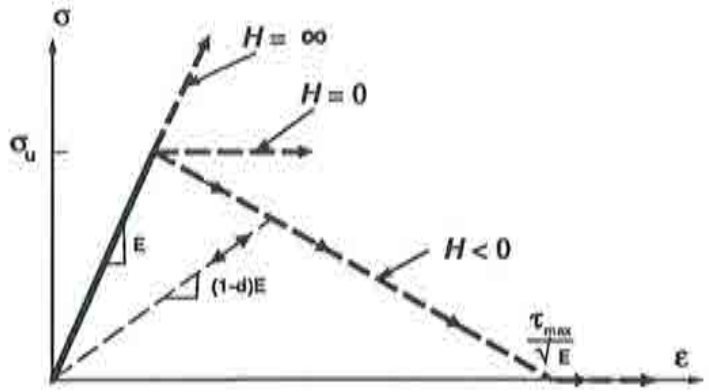

Figure 3. *Damage model: uniaxial stress-strain law.*

In eqs.(4.1.3) τ^ϵ is an appropriate norm of the strains described below, r_0 is an initial threshold value and $G(\cdot)$ is a non-decreasing scalar function such that $G(r_0) = 0$, $G(\infty) \leq 1$ and $G'(\mu) \geq 0 \ \forall \ \mu \in [r_0, \infty)$. The variable r_t describes, at time t, the size of the elastic domain in the strain space E_ϵ defined as :

$$E_\epsilon := \{\epsilon \mid \tau^\epsilon \leq r_t\} \tag{4.1.4}$$

Under such conditions it is straight forward to check that both d and r always increase along time so that:

$$\begin{aligned} \dot{d} &\geq 0 \\ \dot{r} &\geq 0 \end{aligned} \tag{4.1.5}$$

where $\dot{d} = 0$ for unloading and elastic loading whereas $\dot{d} > 0$ corresponds to inelastic loading.

Finally, from eqs.(4.1.1) and (4.1.2) the dissipation $\mathcal{D}$ can be computed as:

$$\mathcal{D} = -\dot{\Psi} + \boldsymbol{\sigma} : \dot{\boldsymbol{\epsilon}} = \dot{d}\, \Psi_0 \ \geq \ 0 \tag{4.1.6}$$

By specialization of the function $G(\cdot)$ and the norm τ^ϵ in eqs.(4.1.3) different qualitative behaviours can be modelled[11]. Some possible choices are given in Appendix I. For the sake of simplicity we will consider in the following a linear strain hardening-softening law with symmetric tension-compression behaviour defined by:

$$\tau^\epsilon = \sqrt{\boldsymbol{\epsilon} : \mathbf{C} : \boldsymbol{\epsilon}} \tag{4.1.7}$$

$$d = G(r) = \begin{cases} 0 & r < r_0 = \sigma_u/\sqrt{E} \\ \dfrac{1}{1+\mathcal{H}}\left(1 - \dfrac{r_0}{r}\right) & r_0 < r < r_{max} = -\dfrac{1}{\mathcal{H}} r_0 \ \ (\mathcal{H} < 0) \\ 1 & r_{max} < r \end{cases} \tag{4.1.8}$$

In eqs.(4.1.8) $\mathcal{H}$ plays the role of hardening-softening parameter, σ_u is the uniaxial peak stress and E is the Young modulus. The corresponding uniaxial stress-strain law is depicted in Fig. 3.

Observe, from eqs.(4.1.2) and (4.1.7), that a new norm τ^σ in the stress domain could have been defined as:

$$\tau^\sigma = \sqrt{\boldsymbol{\sigma} : \mathbf{C}^{-1} : \boldsymbol{\sigma}} = (1-d)\sqrt{\boldsymbol{\epsilon} : \mathbf{C} : \boldsymbol{\epsilon}} = (1-d)\,\tau^\epsilon \tag{4.1.9}$$

For the purposes of this analysis the norm τ^σ is more suitable than τ^ϵ, so that in the following the model will be described in terms of τ^σ keeping in mind that both norms are related through eqs.(4.1.9)

After some algebraic computations, the corresponding incremental stress-strain law can be computed as:

$$\dot{\boldsymbol{\sigma}} = \boldsymbol{\mathcal{C}}^d : \dot{\boldsymbol{\epsilon}} \tag{4.1.10}$$

where $\boldsymbol{\mathcal{C}}^d$ is the tangent constitutive operator computed as:

$$\begin{aligned} &\dot{d} = 0 \ (\textit{unloading}): \quad \boldsymbol{\mathcal{C}}^d = (1-d)\,\mathbf{C} \\ &\dot{d} \neq 0 \quad (\textit{loading}): \quad \boldsymbol{\mathcal{C}}^d = (1-d)\Big[\mathbf{C} - \frac{1}{(1+\mathcal{H})}\,\frac{\tau_0}{(\tau^\sigma)^3}\,\boldsymbol{\sigma}\otimes\boldsymbol{\sigma}\Big] \end{aligned} \tag{4.1.11}$$

Finally, the dissipation can be rewritten in a suitable form as:

$$\mathcal{D} = \frac{1}{2}(\tau^\sigma)^2\,\frac{\partial}{\partial t}\Big(\frac{d}{1-d}\Big) \geq 0 \tag{4.1.12}$$

where the term $\frac{d}{1-d}$ can be expressed, under loading conditions, as:

$$\frac{d}{1-d} = \frac{1}{\mathcal{H}}\,g \tag{4.1.13}$$

$$g(\boldsymbol{\sigma}) = 1 - \frac{r_0}{\tau^\sigma(\boldsymbol{\sigma})} \tag{4.1.14}$$

REMARK 4.1.1.
Observe from eqs.(4.1.9) and (4.1.14) that if the stresses are bounded (and different from zero) so is g. Also observe that negative values of the hardening-softening parameter ($\mathcal{H} < 0 \Longrightarrow$ strain softening) keep the stresses bounded for any value (even unbounded) of the strain field (see Fig. 3 for 1D cases). These facts will be conveniently exploited in next sections.

4.2. Condition I) : Stress boundedness

The constitutive equation (4.1.2) can be conveniently rephrased as:

$$\Big(1 + \frac{d}{1-d}\Big)\,\boldsymbol{\sigma} = \mathbf{C} : \boldsymbol{\epsilon} \tag{4.2.1}$$

and, by substitution of the strain field (2.3) into eq.(4.2.1), we arrive to:

$$\underbrace{\boldsymbol{\sigma}}_{\textit{bounded}} + \frac{d}{1-d}\,\boldsymbol{\sigma} = \underbrace{\mathbf{C} : \bar{\boldsymbol{\epsilon}}}_{\textit{bounded}} + \underbrace{\delta_S\ \mathbf{C} : (\llbracket \mathbf{u} \rrbracket_S \otimes \mathbf{n})^S}_{\textit{unbounded}} \tag{4.2.2}$$

Inspection of eq.(4.2.2) reveals that if we impose the stress field to be bounded, then the first term of the left-hand side is bounded and so is the first term of the right hand side due to the bounded nature of $\bar{\boldsymbol{\varepsilon}}$ (see eq.(2.3)). Moreover, as we are looking for discontinuous solutions of the problem, then $[\![\mathbf{u}]\!]_S \neq 0$ and, thus, the last term of eq.(4.2.2) is unbounded. Finally, in order to the whole equation have mathematical sense, this unbounded term has to be cancelled by some additional unbounded term in eq.(4.2.2) including a delta-function (the only available candidate is $\frac{d}{1-d}$). Since inspection of the term $\frac{d}{1-d}$ in eq.(4.1.13) reveals that g is bounded ‡ (see REMARK 4.1.1) the only feasible possibility is:

$$\frac{1}{\bar{\mathcal{H}}} = \underbrace{\delta_S \frac{1}{\bar{\mathcal{H}}}}_{unbounded} + \underbrace{\frac{1}{\bar{\mathcal{H}}^*}}_{regular} \tag{4.2.3}$$

For the sake of simplicity we will restrict in the following to the particular case $\frac{1}{\bar{\mathcal{H}}^*} = 0$ (the analysis could be continued for the general case but no additional insight in the problem is gained). So that:

$$\frac{1}{\bar{\mathcal{H}}} = \delta_S \frac{1}{\bar{\mathcal{H}}} \tag{4.2.4}$$

Eq.(4.2.4) states a crucial consequence of the stress boundedness requirement, that is: the *distributional character* of the softening parameter $\bar{\mathcal{H}}$ whose inverse has the structure of a delta-function with an intensity given by $\frac{1}{\bar{\mathcal{H}}}$. The parameter $\bar{\mathcal{H}}$ will be termed from now on *the intrinsic softening parameter*.

By substitution of eq.(4.2.4) into eq.(4.1.13) and then in eq.(4.2.2) we arrive to:

$$\underbrace{\left[\boldsymbol{\sigma} - \mathbf{C} : \bar{\boldsymbol{\varepsilon}}\right]}_{=0 \text{ in } \Omega\setminus\mathcal{S}} = \delta_S \underbrace{\left[\mathbf{C} : (\![\mathbf{u}]\!] \otimes \mathbf{n})^S - \frac{1}{\bar{\mathcal{H}}}\, g\, \boldsymbol{\sigma}\right]}_{=0 \text{ in } \mathcal{S}} \tag{4.2.5}$$

In order to eq.(4.2.5) have mathematical sense the underbraced terms of the left and the right hand sides have to cancel at the continuous $(\Omega \setminus \mathcal{S})$ and discontinuous $(\mathcal{S})$ parts of the body, respectively. Thus, the corresponding stress fields emerge from eq.(4.2.5) as:

$$\boldsymbol{\sigma}_{\Omega\setminus\mathcal{S}} = \mathbf{C} : \bar{\boldsymbol{\varepsilon}} \tag{4.2.6}$$

$$\boldsymbol{\sigma}_S = \frac{\bar{\mathcal{H}}}{g(\boldsymbol{\sigma}_S)}\, \mathbf{C} : (\![\mathbf{u}]\!]_S \otimes \mathbf{n})^S \tag{4.2.7}$$

REMARK (4.2.1)
Eq.(4.2.6) states the elastic behaviour in the continuous part of the body in terms of the regular part of the strains $\bar{\boldsymbol{\varepsilon}}$. A non linear behaviour could have been considered by using the whole eq.(4.2.3) instead of the simplified one of eq.(4.2.4).

REMARK (4.2.2)

‡ The case $\boldsymbol{\sigma} = 0$ also applies here since $g\boldsymbol{\sigma}$ can be shown to be bounded in this case.

Eq.(4.2.7) provides a discrete non-linear stress-jump constitutive equation at the interface $\mathcal{S}$ (discontinuity path) which allows the determination of the complete stress tensor on $\mathcal{S}$ in terms of the jump $[\![\mathbf{u}]\!]_s$ and the normal $\mathbf{n}$. *So, unlike what is usual for constitutive equations at discontinuous interfaces, not only the traction vector is involved. Moreover , this* discrete *constitutive equation is* consistent *(emerges naturally from the stress boundedness requirement) with the original* continuous *constitutive equation described in section 4.1. In particular a subset of eqs.(4.2.7) allows the determination of the jump in terms of the stresses at the interface. Choosing an appropriate orthogonal basis formed by the unit vectors* $\mathbf{n}, \mathbf{p}, \mathbf{q}$ $(\mathbf{n}\cdot\mathbf{p} = \mathbf{n}\cdot\mathbf{q} = \mathbf{p}\cdot\mathbf{q} = \mathbf{0})$, *the components of* $[\![\mathbf{u}]\!]_s$ *and* $\boldsymbol{\sigma}_s$ *on this basis are related by (see Appendix II for details):*

$$\begin{bmatrix} [\![\mathbf{u}]\!]_n \\ [\![\mathbf{u}]\!]_p \\ [\![\mathbf{u}]\!]_q \end{bmatrix}_s = \frac{g_s}{\bar{\mathcal{H}}} \frac{1}{E} \begin{bmatrix} \frac{(1+\nu)(1-2\nu)}{1-\nu} & 0 & 0 \\ 0 & 1+\nu & 0 \\ 0 & 0 & 1+\nu \end{bmatrix} \begin{bmatrix} \sigma_{nn} \\ \sigma_{np} \\ \sigma_{nq} \end{bmatrix}_s \tag{4.2.8}$$

$$\sigma_{pp_s} = \sigma_{qq_s} = \frac{\nu}{1-\nu}\sigma_{nn_s} \quad ; \quad \sigma_{pq_s} = 0 \tag{4.2.9}$$

Observe that the appearance of the term $g_s = g(\boldsymbol{\sigma}_s)$ *in eq.(4.2.8) precludes, in general, a linear dependence of the jump with respect to the traction vector* $\boldsymbol{\sigma}_s \cdot \mathbf{n} = [\sigma_{nn}, \sigma_{np}, \sigma_{nq}]^T_s$ *and involves all the components of the stress tensor in the resolved jump*‡.

REMARK (4.2.3)
Eq.(4.2.2) precludes the appearance of the jump in the initial elastic domain $(d = 0)$. *In fact: in this case eq.(4.2.2) reads:*

$$\underbrace{\boldsymbol{\sigma}}_{\text{bounded}} = \underbrace{\mathbf{C} : \bar{\boldsymbol{\epsilon}}}_{\text{bounded}} + \underbrace{\delta_{\mathcal{S}}\ \mathbf{C} : ([\![\mathbf{u}]\!]_s \otimes \mathbf{n})^{\mathcal{S}}}_{\text{unbounded}} \tag{4.2.10}$$

and the stress boundedness requirement forces the unbounded term of eq.(4.2.10) to drop so that $[\![\mathbf{u}]\!]_s = 0$

REMARK (4.2.4)
Observe that the arguments employed to obtain eq.(4.2.7) can be reversed in the following sense: if a) the distributional character of the hardening-softening parameter, eq.(4.2.4), is enforced (consequently the elastic behaviour defined by eq.(4.2.6) is considered in $(\Omega \setminus \mathcal{S})$ *and b) strain-softening is considered for the constitutive behaviour for* $\mathcal{S}$ $(\bar{\mathcal{H}} < 0)$, *then the stresses are bounded both in* $\Omega \setminus \mathcal{S}$ *(since* $\bar{\boldsymbol{\epsilon}}$ *is bounded in eq.(4.2.6)) and in* $\mathcal{S}$ *(see REMARK 4.1.1). Therefore, eq.(4.2.7) automatically fulfills from the imposition of the standard constitutive equation (4.1.2) through consistency of eq.(4.2.5) . This argument reveals crucial to avoid the explicit imposition of eqs.(4.2.7), which are specific (and sometimes difficult to derive) of the considered constitutive equation, and it will be exploited for the numerical simulation of the problem.*

---

‡ *for unloading processes* $(\dot{d} = 0)$ *then* $\dot{g}_s = 0$ *according to eq.(4.1.13) so, in this case, eqs.(4.2.9) are incrementally linear in the traction vector*

4.3. Condition II) : Traction vector continuity

Once determined the stress field in terms of the displacement jump by eqs.(4.2.7), the next step is the determination of the jump itself. The necessary set of equations is obtained by stating that the traction vector at the continuous part of the body $\Omega\backslash\mathcal{S}$ in the neighborhood ‡‡ of $\mathcal{S}$ equals the traction vector at the discontinuity surface i.e.:

$$\boldsymbol{\sigma}_{\Omega\backslash\mathcal{S}}\,|_{\mathbf{x}\in\mathcal{S}}\cdot\mathbf{n} \;=\; \boldsymbol{\sigma}_{\mathcal{S}}\cdot\mathbf{n} \tag{4.3.1}$$

and from eqs.(4.2.6) and (4.2.7):

$$\mathbf{n}\cdot\mathbf{C}\;:\;\bar{\boldsymbol{\epsilon}} \;=\; \frac{\bar{\mathcal{H}}}{g_{\mathcal{S}}}\,\mathbf{n}\cdot\mathbf{C}\;:(\llbracket\mathbf{u}\rrbracket_{\mathcal{S}}\otimes\mathbf{n})^{S} \;=\; \frac{\bar{\mathcal{H}}}{g_{\mathcal{S}}}\,\mathbf{n}\cdot\mathbf{C}\cdot\mathbf{n}\cdot\llbracket\mathbf{u}\rrbracket_{\mathcal{S}} \tag{4.3.2}$$

Finally, solving for the jump in eq.(4.3.2) one arrives to:

$$\begin{aligned}\llbracket\mathbf{u}\rrbracket_{\mathcal{S}} \;&=\; \frac{g(\boldsymbol{\sigma}_{\mathcal{S}}(\llbracket\mathbf{u}\rrbracket_{\mathcal{S}},\mathbf{n}))}{\bar{\mathcal{H}}}\,\mathbf{Q}^{e-1}\cdot\mathbf{n}\cdot\mathbf{C}:\bar{\boldsymbol{\epsilon}}_{\mathcal{S}}\\ \mathbf{Q}^{e} \;&=\; \mathbf{n}\cdot\mathbf{C}\cdot\mathbf{n}\end{aligned} \tag{4.3.3}$$

where $\mathbf{Q}^{e}$ is the so called elastic acoustic tensor[17]

REMARK 4.3.1.
Eq.(4.3.3), in view of eq.(4.2.7), provides the jump $\llbracket\mathbf{u}\rrbracket_{\mathcal{S}}$ in terms of the regular part of the strains $\bar{\boldsymbol{\epsilon}}_{\mathcal{S}}$ and the normal $\mathbf{n}$. Again, it is emphasized that eqs.(4.3.3), dependent on the considered type of constitutive equation, need not to be explicitly derived for simulation purposes. The relevant fact is that the traction vector continuity requirement of eq.(4.3.1) provides the set of equations which determines the jump.

4.4. Condition III) : Identification of the normal

Let us consider any material point P at the discontinuity surface $\mathcal{S}$ and let $t_0 < t$ be the time in which the discontinuity initiates at P (the initiation time) characterized by:

$$\begin{aligned}\llbracket\mathbf{u}\rrbracket(\mathbf{x}_P,t_0) \;&=\; \llbracket\mathbf{u}\rrbracket^{0}_{\mathcal{S}} \;=\; 0\\ \llbracket\dot{\mathbf{u}}\rrbracket(\mathbf{x}_P,t_0) \;&=\; \llbracket\dot{\mathbf{u}}\rrbracket^{0}_{\mathcal{S}} \;\neq\; 0\end{aligned} \tag{4.4.1}$$

Eq.(4.2.7) can be rewritten as:

$$g_{\mathcal{S}}\boldsymbol{\sigma}_{\mathcal{S}} \;=\; \bar{\mathcal{H}}\mathbf{C}\;:(\llbracket\mathbf{u}\rrbracket_{\mathcal{S}}\otimes\mathbf{n})^{S} \tag{4.4.2}$$

and taking time derivatives in eq.(4.4.2) we get:

$$\dot{g}_{\mathcal{S}}\boldsymbol{\sigma}_{\mathcal{S}} \;+\; g_{\mathcal{S}}\dot{\boldsymbol{\sigma}}_{\mathcal{S}} \;=\; \bar{\mathcal{H}}\mathbf{C}\;:(\llbracket\dot{\mathbf{u}}\rrbracket_{\mathcal{S}}\otimes\mathbf{n})^{S} \tag{4.4.3}$$

---

‡‡ no distinction is made between the traction vector at the positive (Ω^{+}) or negative (Ω^{-}) neighborhoods of $\mathcal{S}$, which are assumed to be the same from the balance laws[16].

where the character of material surface of $\mathcal{S}$ has been considered ($\dot{\mathbf{n}} = 0$). Eq.(4.4.3) holds at any time and in particular at the initiation time t_0, where according to eq.(4.4.1)$_1$ $[\![\mathbf{u}]\!]_s^0 = 0$, so that from eq.(4.4.2) $g_s^0 = 0$ and eq.(4.4.3) leads to:

$$\dot{g}_s^0 \boldsymbol{\sigma}_s^0 = \mathcal{H}\mathbf{C} : ([\![\dot{\mathbf{u}}]\!]_s^0 \otimes \mathbf{n})^S \tag{4.4.4}$$

On the other hand at the initiation time $[\![\mathbf{u}]\!]_s^0 = 0$ and $g_s^0 = 0$ so that $\boldsymbol{\epsilon}_s = \bar{\boldsymbol{\epsilon}}_s^0$ and $d^0 = 0$ (see eqs.(2.3) and (4.1.13), respectively) and finally one can write:

$$\boldsymbol{\sigma}_s^0 = \mathbf{C} : \bar{\boldsymbol{\epsilon}}_s^0 \tag{4.4.5}$$

Substituting eq.(4.4.5) into eq.(4.4.4) we arrive to:

$$\mathbf{C} : ([\![\dot{\mathbf{u}}]\!]_s^0 \otimes \mathbf{n})^S = \frac{\dot{g}_s^0}{\mathcal{H}} \boldsymbol{\sigma}_s^0 = \frac{\dot{g}_s^0}{\mathcal{H}} \mathbf{C} : \bar{\boldsymbol{\epsilon}}_s^0 \tag{4.4.6}$$

and premultiplying both sides of eq.(4.4.6) times $\mathbf{C}^{-1}$:

$$([\![\dot{\mathbf{u}}]\!]_s^0 \otimes \mathbf{n})^S = \frac{\dot{g}_s^0}{\mathcal{H}} \bar{\boldsymbol{\epsilon}}_s^0 \tag{4.4.7}$$

Eqs.(4.4.7) provide a set of equations for the determination of both $[\![\dot{\mathbf{u}}]\!]_s^0$ and $\mathbf{n}$. In particular the normal $\mathbf{n}$ can be determined by tacking advantage of the structure of the right-hand-side of eq.(4.4.7). In fact, pre and post multiplying both sides of the equation by *any* vector $\mathbf{t}$ orthogonal to $\mathbf{n}$, the left-hand-side of eq.(4.4.7) cancels so:

$$\mathbf{t} \cdot ([\![\dot{\mathbf{u}}]\!]_s^0 \otimes \mathbf{n})^S \cdot \mathbf{t} = 0 = \frac{\dot{g}_s^0}{\mathcal{H}} \mathbf{t} \cdot \bar{\boldsymbol{\epsilon}}_s^0 \cdot \mathbf{t} \tag{4.4.8}$$

so that:

$$\mathbf{t} \cdot \bar{\boldsymbol{\epsilon}}_s^0 \cdot \mathbf{t} = 0 \qquad \forall\, \mathbf{t} \mid \mathbf{t} \cdot \mathbf{n} = 0 \tag{4.4.9}$$

REMARK (4.4.1)
Eq.(4.4.9) is sufficient for the determination of the normal $\mathbf{n}$ *at any point of* $\mathcal{S}$ *in terms of the regular (bounded) part of the strains* $\bar{\boldsymbol{\epsilon}}_s^0$ *at the initiation time. In particular, for 2D cases, since the normal and tangent vectors can be defined by an inclination angle* θ *with respect to an orthogonal basis* $\hat{\mathbf{e}}_1$ *and* $\hat{\mathbf{e}}_2$ *as:*

$$\begin{aligned} \mathbf{n} &= cos\theta\ \hat{\mathbf{e}}_1 + sin\theta\ \hat{\mathbf{e}}_2 \\ \mathbf{t} &= -sin\theta\ \hat{\mathbf{e}}_1 + cos\theta\ \hat{\mathbf{e}}_2 \end{aligned} \tag{4.4.10}$$

substitution of eq.(4.4.10) into eq.(4.4.9) leads, after some straight forward computations, to the following closed form solution for θ*:*

$$\theta = atan\left[\frac{\bar{\epsilon}_{12}^0 \pm \sqrt{(\bar{\epsilon}_{12}^0)^2 - \bar{\epsilon}_{11}^0\, \bar{\epsilon}_{22}^0}}{\bar{\epsilon}_{11}^0}\right]_s \tag{4.4.11}$$

providing two different possible solutions for the normal. Additional considerations for 2D cases are given in Appendix III.

An alternative, and completely equivalent, way to compute $\mathbf{n}$ emerges from eq.(4.4.6). Multiplying both sides of eq.(4.4.6) by $\bar{\boldsymbol{\epsilon}}_s^0$ and taking into account eq.(4.4.5) we get:

$$\bar{\boldsymbol{\epsilon}}_s^0 : \mathbf{C} \cdot \mathbf{n} \cdot [\![\dot{\mathbf{u}}]\!]_s^0 = \boldsymbol{\sigma}_s^0 \cdot \mathbf{n} \cdot [\![\dot{\mathbf{u}}]\!]_s^0 = \frac{\dot{g}_s^0}{\mathcal{H}} \boldsymbol{\sigma}_s^0 : \mathbf{C}^{-1} : \boldsymbol{\sigma}_s^0 \tag{4.4.12}$$

and thus:

$$\frac{\dot{g}_s^0}{\mathcal{H}} = \frac{\boldsymbol{\sigma}_s^0 \cdot \mathbf{n} \cdot [\![\dot{\mathbf{u}}]\!]_s^0}{\boldsymbol{\sigma}_s^0 : \mathbf{C}^{-1} : \boldsymbol{\sigma}_s^0} \tag{4.4.13}$$

Now, premultiplying both sides of eq.(4.4.6) times $\mathbf{n}$ one gets:

$$\mathbf{n} \cdot \mathbf{C} \cdot \mathbf{n} \cdot [\![\dot{\mathbf{u}}]\!]_s^0 = \frac{\dot{g}_s^0}{\mathcal{H}} \mathbf{n} \cdot \boldsymbol{\sigma}_s^0 \tag{4.4.14}$$

and substituting eq.(4.4.13) into (4.4.14) we arrive to:

$$\mathbf{n} \cdot \mathbf{C} \cdot \mathbf{n} \cdot [\![\dot{\mathbf{u}}]\!]_s^0 - \frac{\mathbf{n} \cdot \boldsymbol{\sigma}_s^0 \otimes \boldsymbol{\sigma}_s^0 \cdot \mathbf{n}}{\boldsymbol{\sigma}_s^0 : \mathbf{C}^{-1} : \boldsymbol{\sigma}_s^0} \cdot [\![\dot{\mathbf{u}}]\!]_s^0 = 0 \tag{4.4.15}$$

Eq.(4.4.15) can we rearranged as follows (see eq.(4.1.9)):

$$\mathbf{Q}_s^{d\,0}(\mathbf{n}) \cdot [\![\dot{\mathbf{u}}]\!]_s^0 = 0 \tag{4.4.16}$$

$$\mathbf{Q}_s^{d\,0}(\mathbf{n}) = \mathbf{n} \cdot \boldsymbol{\mathcal{C}}_s^{d\,0} \cdot \mathbf{n} \tag{4.4.17}$$

$$\boldsymbol{\mathcal{C}}_s^{d\,0} = \mathbf{C} - \frac{\boldsymbol{\sigma}_s^0 \otimes \boldsymbol{\sigma}_s^0}{\boldsymbol{\sigma}_s^0 : \mathbf{C}^{-1} : \boldsymbol{\sigma}_s^0} = \mathbf{C} - \frac{\boldsymbol{\sigma}_s^0 \otimes \boldsymbol{\sigma}_s^0}{(\tau_s^{\sigma\,0})^2} \tag{4.4.18}$$

Inspection of eq.(4.4.18) in comparison to eq.(4.1.11) reveals that $\boldsymbol{\mathcal{C}}_s^{d\,0}$ is the elasto-damage tangent constitutive tensor at the initiation time (when $d = 0$ and $r_0 = \tau^\sigma$) *for a null value of the hardening-softening parameter* $\mathcal{H} = 0$ *(or* $\bar{\mathcal{H}} = 0$*)*. Thus, $\mathbf{Q}_s^{d\,0}$ in eq.(4.4.17) is the elasto-damage acoustic tensor at the initiation time for null softening. The existence of solutions $[\![\dot{\mathbf{u}}]\!]_s^0 \neq \mathbf{0}$ for eq.(4.4.16) implies the singularity of the acoustic tensor, that is:

$$\det\left[\mathbf{Q}_s^{d\,0}(\mathbf{n})\right] = 0 \tag{4.4.19}$$

which con be solved for $\mathbf{n}$.

REMARK (4.4.2)
Observe the similarity of the previous procedure for the determination of $\mathbf{n}$ *with the ones used in failure analysis based on the acoustic tensor*[13]*. It is emphasized, however, that in the present strong discontinuity analysis the considered acoustic tensor corresponds to the initiation time and to a zero value of the softening parameter.*

4.5. Dissipation: the Fracture Energy

From the principle of the expended power, and neglecting the kinetic energy, the external energy supplied to the body along the time interval $[t_1, t_2]$ can be expressed as:

$$\begin{aligned} W_{ext}\Big|_1^2 &= \int_{t_1}^{t_2} \left[\int_\Omega \boldsymbol{\sigma} : \dot{\boldsymbol{\epsilon}} \, d\Omega \right] dt = \int_{t_1}^{t_2} \left[\int_\Omega (\dot{\Psi} + \mathcal{D}) \, d\Omega \right] dt \\ &= \int_\Omega \left[(\Psi_2 - \Psi_1) + \int_{t_1}^{t_2} \mathcal{D} \, dt \right] d\Omega \end{aligned} \tag{4.5.1}$$

where Ψ and $\mathcal{D}$ stand for the Helmholz free energy and the dissipation, respectively, which from eqs.(4.1.1) to (4.1.2) and eqs.(4.1.12) to (4.1.14) can be written as:

$$\Psi = \frac{1}{2} \boldsymbol{\sigma} : \boldsymbol{\epsilon} \tag{4.5.2}$$

$$\mathcal{D} = \frac{1}{2\bar{\mathcal{H}}} (\tau^\sigma)^2 \, \dot{g} = \frac{r_0}{2\bar{\mathcal{H}}} \dot{\tau}^\sigma = \delta_S \frac{r_0}{2\bar{\mathcal{H}}} \dot{\tau}_S^\sigma \tag{4.5.3}$$

Let us imagine the deformation process leading to the formation of the strong discontinuity along $\mathcal{S}$ as follows: the process starts at time $t_0 = 0$ with $(\Psi_0, \tau_0^\sigma, d_0) = (0, 0, 0)$, then the stresses increase elastically (with no dissipation) until the initial threshold value r_0 is reached at time t_1 when $(\Psi_1, \tau_1^\sigma, d_1) = (\frac{1}{2} r_0^2, r_0, 0)$. Finally a monotonic loading process ($\dot{d} \neq 0$) is driven up to the total stress relaxation at time t_2 with $(\Psi_2, \tau_2^\sigma, d_2) = (0, 0, 1)$. According to eqs.(4.5.1) and (4.5.3) the external energy supplied along the process can be computed as:

$$\begin{aligned} W_{ext}\Big|_0^2 &= \int_\Omega \left[(\underbrace{\Psi_2}_{=0} - \underbrace{\Psi_0}_{=0}) + \int_{t_1}^{t_2} \mathcal{D} \, dt \right] d\Omega = \int_{t_1}^{t_2} \left[\int_\Omega \delta_S \frac{r_0}{2\bar{\mathcal{H}}} \dot{\tau}_S^\sigma \, d\Omega \right] dt \\ &= \int_{t_1}^{t_2} \left[\int_\mathcal{S} \frac{r_0}{2\bar{\mathcal{H}}} \dot{\tau}_S^\sigma \, d\Gamma \right] dt = \int_\mathcal{S} \frac{r_0}{2\bar{\mathcal{H}}} \left[\int_{\tau_1^\sigma}^{\tau_2^\sigma} d\tau^\sigma \right] d\Gamma \\ &= \int_\mathcal{S} \frac{r_0}{2\bar{\mathcal{H}}} \left[\underbrace{\tau_2^\sigma}_{=0} - \underbrace{\tau_1^\sigma}_{=r_0} \right] d\Gamma = \int_\mathcal{S} -\frac{{r_0}^2}{2\bar{\mathcal{H}}} d\Gamma \end{aligned} \tag{4.5.4}$$

Thus, the kernel of the last integral in eq.(4.5.4) corresponds to the supplied energy per unit surface of the discontinuity path $\mathcal{S}$, which can be immediately identified as the so called *fracture energy* G_f, that is:

$$G_f = -\frac{{r_0}^2}{2\bar{\mathcal{H}}} \tag{4.5.5}$$

and considering eq.(4.1.8.a), eq.(4.5.5) can be solved for $\bar{\mathcal{H}}$:

$$\bar{\mathcal{H}} = -\frac{r_0^2}{2G_f} = -\frac{{\sigma_u}^2}{2G_f E} \tag{4.5.6}$$

which states that *the intrinsic softening parameter $\bar{\mathcal{H}}$ is a material property* related to the fracture energy G_f, Young modulus E and uniaxial peak stress σ_u through eq.(4.5.6). The negative value of $\bar{\mathcal{H}}$ is also stated there.

5. STRONG DISCONTINUITY ANALYSIS FOR PLASTICITY MODELS

5.1. A plasticity model with strain softening

We now consider the family of elasto-plasticity models. For the sake of simplicity we will restrict to the classical associative rate-independent model defined by:

$$\dot{\boldsymbol{\sigma}} = \mathbf{C} : (\dot{\boldsymbol{\epsilon}} - \dot{\boldsymbol{\epsilon}}^p) \tag{5.1.1}$$

$$\dot{\boldsymbol{\epsilon}}^p = \lambda \frac{\partial \phi}{\partial \boldsymbol{\sigma}} \tag{5.1.2}$$

$$\dot{q} = -\lambda \mathcal{H} \frac{\partial \phi}{\partial q} \tag{5.1.3}$$

$$\phi(\boldsymbol{\sigma}, q) = \hat{\phi}(\boldsymbol{\sigma}) + q - \sigma_y \tag{5.1.4}$$

$$\lambda \geq 0 \qquad \phi(\boldsymbol{\sigma}, q) \leq 0 \qquad \lambda\, \phi(\boldsymbol{\sigma}, q) = 0 \tag{5.1.5}$$

where $\boldsymbol{\sigma}$, $\boldsymbol{\epsilon}$ and $\boldsymbol{\epsilon}^p$ are the stress, strain and plastic strain tensors, respectively, $\mathbf{C}$ is the isotropic elastic constitutive tensor, q is the stress-like internal variable, $\hat{\phi}(\boldsymbol{\sigma})$ is an homogeneous (degree one) function, $\sigma_y > 0$ is the flow stress and $\mathcal{H}$ is the softening parameter assumed to be negative ($\mathcal{H} < 0$). Eqs.(5.1.5) are the classical Kuhn-Tucker conditions allowing for the determination of the plastic multiplier λ which can be computed from the consistency condition $\dot{\phi} = 0$, in terms of $\dot{\boldsymbol{\sigma}}$ or $\dot{\boldsymbol{\epsilon}}$, as:

$$\lambda = \frac{1}{\mathcal{H}} \frac{\partial \hat{\phi}}{\partial \boldsymbol{\sigma}} : \dot{\boldsymbol{\sigma}} = \frac{1}{\mathcal{H}} \nabla \hat{\phi} : \dot{\boldsymbol{\sigma}} = -\frac{1}{\mathcal{H}} \dot{q} \tag{5.1.6}$$

$$\lambda = \frac{\nabla \hat{\phi} : \mathbf{C}}{\mathcal{H} + \nabla \hat{\phi} : \mathbf{C} : \nabla \hat{\phi}} : \dot{\boldsymbol{\epsilon}} \tag{5.1.7}$$

Substitution of eqs.(5.1.6) and (5.1.7) into eq.(5.1.1) leads to the classical elastoplastic tangent constitutive tensor $\boldsymbol{\mathcal{C}}^{ep}$ defined by:

$$\dot{\boldsymbol{\sigma}} = \boldsymbol{\mathcal{C}}^{ep} : \dot{\boldsymbol{\epsilon}} \tag{5.1.8}$$

$$\boldsymbol{\mathcal{C}}^{ep} = \mathbf{C} - \frac{\mathbf{C} : \nabla \hat{\phi} \otimes \nabla \hat{\phi} : \mathbf{C}}{\mathcal{H} + \nabla \hat{\phi} : \mathbf{C} : \nabla \hat{\phi}} \tag{5.1.9}$$

and, conversely, the elastoplastic compliance constitutive tensor $\boldsymbol{\mathcal{C}}^{ep-1}$ can be defined as:

$$\dot{\boldsymbol{\epsilon}} = \boldsymbol{\mathcal{C}}^{ep-1} : \dot{\boldsymbol{\sigma}} \tag{5.1.10}$$

$$\boldsymbol{\mathcal{C}}^{ep-1} = \mathbf{C}^{-1} + \frac{1}{\mathcal{H}} \nabla \hat{\phi} \otimes \nabla \hat{\phi} \tag{5.1.11}$$

Finally, the dissipation $\mathcal{D}$ can be computed as:

$$\mathcal{D} = \sigma_y \lambda = -\frac{1}{\mathcal{H}} \sigma_y \dot{q} \geq 0 \tag{5.1.12}$$

5.2. Condition I): Stress boundedness

Taking time derivatives of eq.(2.3) and considering the material surface character of the discontinuity surface $\mathcal{S}$ ($\dot{\mathbf{n}} = 0$) we arrive to:

$$\dot{\boldsymbol{\epsilon}} \;=\; \dot{\tilde{\boldsymbol{\epsilon}}} + \delta_{\mathcal{S}}\,(\llbracket \dot{\mathbf{u}} \rrbracket \otimes \mathbf{n})^{S} \tag{5.2.1}$$

and substituting eq.(5.2.1) into eq.(5.1.10) and then into eq.(5.1.11):

$$\underbrace{\dot{\tilde{\boldsymbol{\epsilon}}}}_{bounded} + \underbrace{\delta_{\mathcal{S}}\,(\llbracket \dot{\mathbf{u}} \rrbracket_{s} \otimes \mathbf{n})^{S}}_{unbounded} \;=\; \underbrace{\mathbf{C}^{-1} : \dot{\boldsymbol{\sigma}}}_{bounded} + \frac{1}{\mathcal{H}}\,\underbrace{\nabla\dot{\phi} \otimes \nabla\dot{\phi} : \dot{\boldsymbol{\sigma}}}_{bounded} \tag{5.2.2}$$

If we require the stress field $\boldsymbol{\sigma}$ (and also $\dot{\boldsymbol{\sigma}}$) to be bounded, the unbounded term of the left-hand-side of eq.(5.2.2) needs to be canceled in order to $\llbracket \dot{\mathbf{u}} \rrbracket_{s}$ be non zero. In view of eqs.(5.2.2) this cancelation can only be achieved if a delta-function appears in the structure of $\frac{1}{\mathcal{H}}$ so that:

$$\frac{1}{\mathcal{H}} \;=\; \delta_{\mathcal{S}}\,\frac{1}{\bar{\mathcal{H}}} + \frac{1}{\mathcal{H}^{*}} \tag{5.2.3}$$

As in section 4.2 we will consider the simplest case ($\frac{1}{\mathcal{H}^{*}} = 0$) so that:

$$\frac{1}{\mathcal{H}} \;=\; \delta_{\mathcal{S}}\,\frac{1}{\bar{\mathcal{H}}} \tag{5.2.4}$$

from which the distributional character of the softening parameter $\mathcal{H}$ emerges in terms of the *intrinsic softening parameter* $\bar{\mathcal{H}}$.

Now, substituting eq.(5.2.4) into eq.(5.2.2) and cancelling the bounded terms in the continuous domain $\Omega\backslash\mathcal{S}$ and the unbounded terms in the discontinuity surface $\mathcal{S}$ we arrive to:

$$\dot{\tilde{\boldsymbol{\epsilon}}} \;=\; \mathbf{C}^{-1} : \dot{\boldsymbol{\sigma}}_{\Omega\backslash\mathcal{S}} \Longrightarrow \dot{\boldsymbol{\sigma}}_{\Omega\backslash\mathcal{S}} \;=\; \mathbf{C} : \dot{\tilde{\boldsymbol{\epsilon}}} \tag{5.2.5}$$

$$(\llbracket \dot{\mathbf{u}} \rrbracket_{s} \otimes \mathbf{n})^{S} \;=\; \frac{1}{\bar{\mathcal{H}}}\,\nabla\dot{\phi}_{s} \otimes \nabla\dot{\phi}_{s} : \dot{\boldsymbol{\sigma}}_{s} \tag{5.2.6}$$

Eq.(5.2.5) states the elastic stress-strain behaviour at the continuous part ($\Omega\backslash\mathcal{S}$) of the body. Eq.(5.2.6) provides a discrete constitutive equation at the discontinuity surface $\mathcal{S}$ consistent with the original elasto-plastic constitutive equation given by eqs.(5.1.1) to (5.1.5). It relates the displacement jump rate $\llbracket \dot{\mathbf{u}} \rrbracket_{s}$ the stresses $\boldsymbol{\sigma}_{s}$ and the stress rates $\dot{\boldsymbol{\sigma}}_{s}$ at the discontinuity interface $\mathcal{S}$.

REMARK (5.2.1)
The same comments than in REMARK(4.2.4) are applicable here. So, if a) eq.(5.2.4) (distributional character of the hardening parameter) and consequently eq.(5.2.5) (elastic stress-strain behaviour in $\Omega\backslash\mathcal{S}$) are enforced, and b) the stresses are bounded in $\mathcal{S}$ (by imposing a negative value of $\bar{\mathcal{H}}$) (strain-softening) then eqs.(5.2.6) need not to be explicitely imposed and they are implicitely fulfilled from the elasto-plastic constitutive equation (5.1.10) and eqs.(5.2.2).

REMARK (5.2.2)
A subset of eqs.(5.2.6) provides the resolved rate of the jump $[\![\dot{\mathbf{u}}]\!]_S$ in terms of $\dot{\boldsymbol{\sigma}}_S$ (see Appendix II for details). For the particular case of the J_2 flow theory and 2D cases, the results can be very simplified leading to:

$$\begin{aligned} [\![\dot{\mathbf{u}}]\!]_{n_S} &= 0 \\ [\![\dot{\mathbf{u}}]\!]_{p_S} &= \dot{\gamma}_S = \frac{3}{\bar{\mathcal{H}}}\,\dot{\tau}_S \end{aligned} \tag{5.2.7}$$

where $[\![\mathbf{u}]\!]_{n_S}$ and $[\![\mathbf{u}]\!]_{p_S} = \gamma_S$ are the normal and the tangential components of the displacement jump, respectively, and τ_S is the shear stress along the discontinuity line $\mathcal{S}$. Therefore, eqs.(5.2.7) state that using the J_2 flow theory only slip lines ($[\![\dot{\mathbf{u}}]\!]_n = 0$), ruled by the simple discrete stress-displacement eq.(5.2.7.b), can be modelled.

5.3. Condition II): Traction vector continuity

Traction vector continuity across $\mathcal{S}$ reads

$$\boldsymbol{\sigma}_{\Omega\setminus\mathcal{S}}\,|_{\mathbf{x}\in\mathcal{S}}\cdot\mathbf{n} = \boldsymbol{\sigma}_S\cdot\mathbf{n} \tag{5.3.1}$$

or, taking time derivatives in eq.(5.3.1) (and considering $\dot{\mathbf{n}} = 0$):

$$\dot{\boldsymbol{\sigma}}_{\Omega\setminus\mathcal{S}}\,|_{\mathbf{x}\in\mathcal{S}}\cdot\mathbf{n} = \dot{\boldsymbol{\sigma}}_S\cdot\mathbf{n} \tag{5.3.2}$$

Unlike in damage models, eq. (5.2.6) can not be explicitely inverted, to solve for $\dot{\boldsymbol{\sigma}}_S$, due to the incomplete range of the fourth order tensor $\nabla\dot{\phi}_S\otimes\nabla\dot{\phi}_S$. The full determination of the stress field has to be done in conjunction with the equations provided by the traction vector continuity requirement so that, finally, eqs.(5.2.6) and (5.3.1) or (5.3.2) provide a well posed, in general nonlinear, system of equations allowing for the determination of the jump $[\![\mathbf{u}]\!]_S$ and the stress field $\boldsymbol{\sigma}_S$ at the discontinuity surface.

5.4. Condition III): Identification of the normal

According to eqs.(4.4.1) and (2.3) at the initiation time $\boldsymbol{\epsilon}^0 = \bar{\boldsymbol{\epsilon}}^0_S$ so that:

$$\boldsymbol{\sigma}^0_S = \boldsymbol{\sigma}(\bar{\boldsymbol{\epsilon}}^0_S) \tag{5.4.1}$$

and eqs.(5.2.6) can be written at the initiation time t_0 as:

$$\begin{aligned} ([\![\dot{\mathbf{u}}]\!]^0_S\otimes\mathbf{n})^S &= \gamma^0\,\nabla\dot{\phi}(\boldsymbol{\sigma}^0_S) = \gamma^0\,\nabla\dot{\phi}^0(\bar{\boldsymbol{\epsilon}}^0_S) \\ \gamma^0 &= \frac{\nabla\dot{\phi}^0_S : \dot{\boldsymbol{\sigma}}^0_S}{\bar{\mathcal{H}}} = \frac{\dot{\phi}^0_S}{\bar{\mathcal{H}}} \end{aligned} \tag{5.4.2}$$

Observe that in eq.(5.4.2) $\nabla\dot{\phi}^0$ can be computed, through eqs.(5.4.1), in terms of the bounded part of the strain at the initiation time, $\bar{\boldsymbol{\epsilon}}^0_S$. Eq.(5.4.2) provides a set of equations similar to the ones obtained for the damage model (see eq.(4.4.7)).

Thus, a similar procedure to the one explained in section 4.4 can be applied here for the obtention of $\mathbf{n}$ leading to:

$$\mathbf{t} \cdot \nabla \hat{\phi}_s^0 \cdot \mathbf{t} = 0 \qquad \forall\, \mathbf{t} \;\mid\; \mathbf{t} \cdot \mathbf{n} = 0 \tag{5.4.3}$$

As said in REMARK(4.4.1), for 2D cases the inclination angle θ of the normal with respect to an orthogonal basis $\hat{\mathbf{e}}_1, \hat{\mathbf{e}}_2$ can be explicitely computed in terms of the components of $\nabla \hat{\phi}_s^0$ as:

$$\theta \;=\; atan\left[\frac{\nabla \hat{\phi}_{12}^0 \;\pm\; \sqrt{(\nabla \hat{\phi}_{12}^0)^2 \;-\; \nabla \hat{\phi}_{11}^0 \;\nabla \hat{\phi}_{22}^0}}{\nabla \hat{\phi}_{11}^0}\right]_s \tag{5.4.4}$$

For the particular case of J2 flow theory and 2D (plane-strain, plane-stress) cases it can be shown (see Appendix III, section III.2) that the inclination angle of the normal *with respect to the maximum principal stress* is $\theta = \pm\frac{\pi}{4}$.

An alternative procedure for the computation of $\mathbf{n}$ can be obtained following the same steps than in section 4.4. for the damage model: multiplying both sides of eq.(5.4.2.a) times $\nabla \hat{\phi}_s^0 : \mathbf{C}$ we get:

$$\nabla \hat{\phi}_s^0 : \mathbf{C} \;:\; (\llbracket \dot{\mathbf{u}} \rrbracket_s^0 \otimes \mathbf{n})^S \;=\; \gamma^0\, \nabla \hat{\phi}^0 : \mathbf{C} : \nabla \hat{\phi}_s^0$$

thus,

$$\gamma^0 \;=\; \frac{\nabla \hat{\phi}_s^0 : \mathbf{C} \cdot \llbracket \dot{\mathbf{u}} \rrbracket_s^0 \cdot \mathbf{n}}{\nabla \hat{\phi}_s^0 : \mathbf{C} : \nabla \hat{\phi}_s^0} \tag{5.4.5}$$

Now, multiplying eq.(5.4.2.a) times $\mathbf{n} \cdot \mathbf{C}$ we obtain:

$$\mathbf{n} \cdot \mathbf{C} \;:\; (\llbracket \dot{\mathbf{u}} \rrbracket_s^0 \otimes \mathbf{n}) \;=\; \mathbf{n} \cdot \mathbf{C} \cdot \mathbf{n} \cdot \llbracket \dot{\mathbf{u}} \rrbracket_s^0 \;=\; \mathbf{n} \cdot \mathbf{C} : \nabla \hat{\phi}_s^0\, \gamma^0 \tag{5.4.6}$$

and substituting eq.(5.4.5) into (5.4.6) we arrive to:

$$\mathbf{n} \cdot \mathbf{C} \cdot \mathbf{n} \cdot \llbracket \dot{\mathbf{u}} \rrbracket_s^0 \;-\; \mathbf{n} \cdot \frac{\mathbf{C} : \nabla \hat{\phi}_s^0 \otimes \nabla \hat{\phi}_s^0 : \mathbf{C}}{\nabla \hat{\phi}_s^0 : \mathbf{C} : \nabla \hat{\phi}_s^0} \cdot \mathbf{n} \cdot \llbracket \dot{\mathbf{u}} \rrbracket_s^0 \;=\; \mathbf{0} \tag{5.4.7}$$

Eq.(5.4.7) can be rearranged as follows:

$$\mathbf{Q}_s^{ep0}(\mathbf{n}) \cdot \llbracket \dot{\mathbf{u}} \rrbracket_s^0 \;= \mathbf{0} \tag{5.4.8}$$

$$\mathbf{Q}_s^{ep0}(\mathbf{n}) \;=\; \mathbf{n} \cdot \boldsymbol{\mathcal{C}}_s^{ep0} \cdot \mathbf{n} \tag{5.4.9}$$

$$\boldsymbol{\mathcal{C}}_s^{ep0} \;=\; \mathbf{C} - \frac{\mathbf{C} : \nabla \hat{\phi}_s^0 \otimes \nabla \hat{\phi}_s^0 : \mathbf{C}}{\nabla \hat{\phi}_s^0 : \mathbf{C} : \nabla \hat{\phi}_s^0} \tag{5.4.10}$$

The existence of solutions $\llbracket \dot{\mathbf{u}} \rrbracket_s^0 \neq 0$ in eq.(5.4.8) implies the singularity of the elastoplastic acoustic tensor $\mathbf{Q}_s^{ep0}(\mathbf{n})$, so that:

$$\det\left[\mathbf{Q}_s^{ep0}(\mathbf{n})\right] \;=\; 0 \tag{5.4.11}$$

from which $\mathbf{n}$ can be computed. Observe in eqs.(5.4.9) and (5.4.10) that $\mathbf{Q}_s^{ep0}$ is given in terms of $\boldsymbol{\mathcal{C}}_s^{ep0}$ which is the elastoplastic tangent constitutive tensor at the initiation time *with null hardening* as can be checked by comparison with eq.(5.1.9).

5.5. Dissipation: the Fracture Energy

From eq.(5.1.12) and taking into account eq.(5.2.4) the dissipation can be written as:

$$\mathcal{D} \;=\; -\frac{1}{\bar{\mathcal{H}}}\,\sigma_y\,\dot{q} \;=\; -\delta_S\,\frac{1}{\bar{\mathcal{H}}}\,\sigma_y\,\dot{q} \tag{5.5.1}$$

where, during plastic loading, q can be computed from the consistency equation $\phi(\boldsymbol{\sigma}, q) = 0$ and, consequently, from eq.(5.1.4):

$$q \;=\; \sigma_y - \hat{\phi}(\boldsymbol{\sigma}) \tag{5.5.2}$$

Notice that $\hat{\phi}(\mathbf{0}) = 0$ due to the homogeneous character of the function $\hat{\phi}(\cdot)$. On the other hand the free energy can be expressed, considering eq.(5.2.4), as:

$$\Psi \;=\; \frac{1}{2}\,\boldsymbol{\sigma} : \boldsymbol{C}^{-1} : \boldsymbol{\sigma} + \frac{1}{2}\,\frac{q^2}{\bar{\mathcal{H}}} \;=\; \frac{1}{2}\,\boldsymbol{\sigma} : \boldsymbol{C}^{-1} : \boldsymbol{\sigma} + \frac{1}{2}\,\delta_S \frac{q^2}{\bar{\mathcal{H}}} \tag{5.5.3}$$

Like in section 4.5 let us consider the deformation process leading to the formation of the strong discontinuity as follows: the process starts at time $t_0 = 0$, with $(\Psi_0, q_0) = (0, 0)$. Then the strains are elastically increased (with no dissipation) up to the initiation of the plastic flow at time t_1 (the initiation time). Beyond this point the strain-softening constitutive equation leads to the full relaxation of the stresses at time t_2 where $\hat{\phi}(\boldsymbol{\sigma}_2) = \hat{\phi}(\mathbf{0}) = 0$ and thus $q_2 = \sigma_y$ from eq.(5.5.2). Consequently $(\Psi_2, q_2) = (\frac{1}{2}\delta_S \frac{\sigma_y^2}{\bar{\mathcal{H}}}, \sigma_y)$. The externally supplied energy can be then expressed from eq.(4.5.1) as:

$$\begin{aligned} W_{ext}\Big|_0^2 \;&=\; \int_\Omega \Big[(\Psi_2 - \Psi_0) \;+\; \int_{t_1}^{t_2} \mathcal{D}\; dt\Big]\; d\Omega \\ &=\; \int_\Omega \delta_S \Big[\frac{1}{2}\,\frac{\sigma_y^2}{\bar{\mathcal{H}}} - \int_{t_1}^{t_2} \frac{\sigma_y}{\bar{\mathcal{H}}}\,\dot{q}\; dt\Big]\, d\Omega \;=\; \int_S \Big[\frac{1}{2}\,\frac{\sigma_y^2}{\bar{\mathcal{H}}} - \int_{t_1}^{t_2} \frac{\sigma_y}{\bar{\mathcal{H}}}\,\dot{q}\; dt\Big]\, d\Gamma \\ &=\; \int_S \Big[\frac{1}{2}\,\frac{\sigma_y^2}{\bar{\mathcal{H}}} - \frac{\sigma_y}{\bar{\mathcal{H}}} \int_{q_1=0}^{q_2=\sigma_y} dq\Big]\, d\Gamma \;=\; \int_S -\frac{1}{2}\,\frac{\sigma_y^2}{\bar{\mathcal{H}}}\, d\Gamma \end{aligned} \tag{5.5.4}$$

Then the supplied energy per unit of discontinuity surface (*the fracture energy*) can be identified from eq.(5.5.4) as the kernel of the last integral, i.e.:

$$G_f \;=\; -\frac{1}{2}\,\frac{{\sigma_y}^2}{\bar{\mathcal{H}}} \tag{5.5.5}$$

Notice again the similarity of eq.(4.5.5) (damage model) with eq.(5.5.5) (plasticity model). From eq.(5.5.5) the intrinsic softening parameter $\bar{\mathcal{H}}$ can be regarded as a material property related to the fracture energy G_f and the flow stress σ_y by:

$$\bar{\mathcal{H}} \;=\; -\frac{1}{2}\,\frac{{\sigma_y}^2}{G_f} \tag{5.5.6}$$

6. CONCLUDING REMARKS

Along the preceding sections, the methodology of application of the strong discontinuity analysis to standard (local, stress-strain) constitutive equations has been presented. The analysis defines a common framework, in which different families of constitutive equations can be inscribed. By imposing several requeriments on the stress field, in order to make the constitutive equation *compatible* with the appearence of strong discontinuities, the analysis provides a set of equations which allows to solve for the additional unknowns appearing in the problem: the displacement jump, the stress field at the discontinuity path and the normal. As main ingredients of the resulting framework, the following should be mentionned:

- The *distributional character of the softening parameter*. On one side, strain-softening has to be considered for the constitutive equation at the discontinuity path. The inverse of the softening parameter must have the structure of a delta function according to eqs.(4.2.4) and (5.2.4) so that, roughly speaking, a perfect-damage or perfect-plasticity behaviour has to be approached from the *softening part* in the constitutive equation. The intensity ot the softening parameter function can be defined in terms of an *intrinsic softening paramter* $\bar{\mathcal{H}}$ *which can be proved to be a material property related to the fracture energy* as shown in eqs.(4.5.6) and (5.5.6). On the other hand an elastic (or, in the most general context, strain-hardening) behaviour has to be considered for the constitutive equation at the continuous part of the body. Under these conditions a consistent *discrete* constitutive equation emerges which relates the stress field at the discontinuity path with the jump. Howewer, this discrete constitutive equation has not necessarly to be explicitely computed for the different constitutive models.

- The *traction vector continuity* condition provides the necessary set of additional equations to determine the jump and the stress field at the discontinuity path. Although explicit expressions for both fields can be sometimes derived, the relevant fact is the necessity of imposition of such condition in the context of strong discontinuity problems.

- The normal to the discontinuity path can be determined by imposition of the material surface character of the discontinuity surface at the initiation time), this leading to very simple expressions, in terms of the regular strain field, which, howewer, have to be specifically determined for each familly of constitutive equations.

This general framework plays a crucial role in the design of appropriate numerical approaches to the strong discontinuity problems. This subjet will be addressed in Part II of this work.

REFERENCES

[1] BELYTSCHKO T., FISH J. and ENGELMANN B.E. A finite element with embedded localization zones. Comp. Meth. Appl. Mech. Engng., 70, 59-89, 1988

[2] De BORST R., MUHLHAUS H.B., PAMIN J., and SLUYS L.J. Computational Modelling of Localisation of Deformation. In: D.R.J. Owen et. al., editors, *Proc. of the Third Conference on Computational Plasticity: Fundamentals and Applications*, 483-508, Pineridge Press, Swansea, 1992

[3] DVORKIN E.N., CUITIÑO A.M and GIOIA G. Finite elements with displacement interpolated embedded localization lines insensitive to mesh size and distortions. Int. Journ. Num. Meth. Engng., 30, 541-564, 1990

[4] HILLERBORG A. Numerical methods to simulate softening and fracture of concrete. In: G.C. Sih and A. Di Tomaso editors, *Fracture Mechanics of Concrete: Structural Application and Numerical Calculation*, 141-170, 1985

[5] LARSSON. R. RUNESSON K. and OTTOSEN N.S. Discontinuous displacement approximation for capturing plastic localization. Int. Journ. Num. Meth. Engng., 36, 2087-2105, 1993

[6] LOFTI H.R. and SHING P.B. Analysis of concrete fracture with an embedded crack approach. In: H. Mang et. al., editors, *Proc. EURO-C 1994 Computer Modelling of concrete structures*, 343-352, Pineridge Press, Swansea, 1994

[7] MAMIYA E. and SIMO J.C. Numerical analysis of equilibrium shocks and phase transitions in non linear elasticity. Journal of Elasticity, 1994

[8] NEEDLEMAN A. Material Rate Dependence and Mesh Sensitivity in Localization Problems. Comp. Meth. Appl. Mech. Engng., 67, 69-86, 1988

[9] OLIVER J. A consistent characteristic length for smeared cracking models. Int. Journ. Num. Meth. Engng., 28, 461-474, 1989

[10] OLIVER J. Continuum modelling of strong discontinuities in solid mechanics. In: D.R.J. Owen et. al., editors, *Proc. COMPLAS IV, Fourth international conference on computational plasticity*,455-479 , Pineridge Press, Swansea, 1995

[11] OLIVER J., CERVERA M., OLLER S. and LUBLINER J. Isotropic damage models and smeared crack analysis of concrete. In: N. Bicanic et. al., editors, *Proc. SCI-C Computer Aided Analysis and Design of Concrete Structures*, 945-957, Pineridge Press, Swansea, 1990

[12] OLIVER J. and SIMO J.C. Modelling strong discontinuities by means of strain softening constitutive equations. In: H. Mang et. al., editors, *Proc. EURO-C 1994 Computer Modelling of concrete structures*, 363-372, Pineridge Press, Swansea, 1994

[13] OTTOSEN N.S. and RUNESSON K. Properties of discontinuous bifurcation solutions in elasto-plasticity. Int. J. Solids Structures, Vol. 27, No. 4,p.p 401-421, 1991

[14] PIJAUDIER CABOT G. and BAZANT Z.P. Nonlocal Damage Theory. Jour. Engng. Mech., A.S.C.E., 113, 1512-1533, 1987

[15] SIMO J.C., OLIVER J. and ARMERO F. An analysis of strong discontinuities induced by strain-softening in rate-independent inelastic solids. Computational Mechanics, 12, 277-296, 1993

[16] SIMO J.C. and OLIVER J. A new approach to the analysis and simulation of strong discontinuities. In: Z.P. Bazant et. al., editors, *Fracture and Damage in Quasibrittle Structures*, 25-39, E & FN Spon, 1994

[17] WILLAM K. and SOBH N. Bifurcation analysis of tangential material operators. In: G.N. Pande et. al., editors, *Proc. NUMETA-87 Transient/Dynamic Analysis of Constitutive Laws for Engineering Materials*, C4/1-C4/13, Martinus Nijhoff Publishers, Dordrecht, 1987

[18] ZIENKIEWICZ O.C., HUANG M. and PASTOR M. Localization problems in plasticity using finite elements with adaptive remeshing. Int. Journ. Num. Meth. Engng., 19, 127-148, 1995

APPENDIX I
SOME ALTERNATIVES FOR THE CONTINUUM DAMAGE MODEL

a) Non symmetric tension-compression behaviour

The strain norm r^ϵ in eq.(4.1.7) can be rewritten in terms of the so called *effective stress* $\bar{\sigma} = \mathbf{C} : \boldsymbol{\epsilon}$ as:

$$r^\epsilon = \sqrt{\bar{\sigma} : \epsilon} \tag{I.1}$$

The corresponding damage model is symmetric in the tension-compression domains as can be checked in Figs. 4a and 4b. A more realistic approach for many geomaterials, in which the maximum compressive strength is much higher than the maximun tensile strength, can be obtained by modifying eq.(I.1) as follows[11]:

$$\tilde{r}^\epsilon = \sqrt{\sum_i^3 < \bar{\sigma}_i > \epsilon_i} \tag{I.2}$$

where $\bar{\sigma}_i$ and ϵ_i are the principal stress and strain components, respectively and $< \cdot >$ is the Mc. Auley bracket. Due to the isotropic character of the elastic tensor $\mathbf{C}$, the principal directions of both tensors coincide. The corresponding initial elastic domain, in the principal stress space, and the uniaxial stress-strain law are depicted in Figs. 4c and 4d, respectively. Observe that this domain is open in the pure compression octant which guaranties a linear elastic behaviour in this domain.

b) Exponential softening

Eq.(4.1.8)$_2$ define a linear strain-softening law (see Fig. 4e). An alternative exponential softening law can be defined as[11]:

$$d = G(r) = 1 - \frac{r_0}{r} e^{\mathcal{H}(\frac{r}{r_0} - 1)} \tag{I.3}$$

where $\mathcal{H}$ plays the role of softening parameter ($\mathcal{H} < 0$). The corresponding uniaxial stres-strain law is depicted in Fig. 4f.

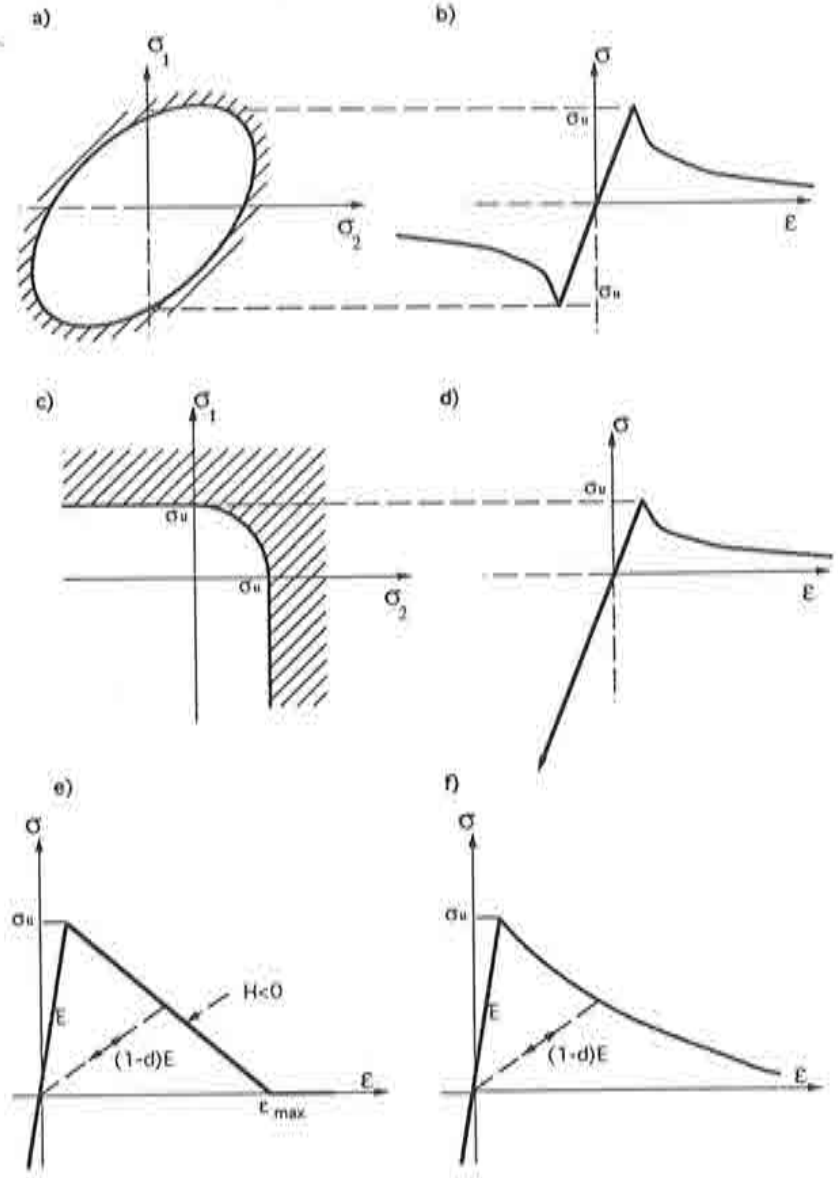

Figure 4. *Different alternatives for the continuum damage model.*

APPENDIX II
RESOLVED JUMPS

Let us consider the equation:

$$([\![\mathbf{u}]\!] \otimes \mathbf{n})^S = \mathbf{A} \qquad \mathbf{A}^T = \mathbf{A} \tag{II.1}$$

and the orthogonal basis constituted by $\mathbf{n}$ any two (mutually orthogonal) unit vectors $\mathbf{p}$ and $\mathbf{q}$ such that:

$$\mathbf{n}\cdot\mathbf{p} = \mathbf{n}\cdot\mathbf{q} = \mathbf{p}\cdot\mathbf{q} = 0 \qquad |\mathbf{n}| = |\mathbf{p}| = |\mathbf{q}| = 1 \tag{II.2}$$

Let:

$$\begin{bmatrix} A_{nn} & A_{np} & A_{nq} \\ A_{np} & A_{pp} & A_{pq} \\ A_{nq} & A_{pq} & A_{qq} \end{bmatrix} \tag{II.3}$$

be the matrix of components of $\mathbf{A}$ in the chosen basis. It is straight forward to check that the following relations hold:

$$A_{pp} = \mathbf{p}\cdot\mathbf{A}\cdot\mathbf{p} = \mathbf{p}\cdot([\![\mathbf{u}]\!] \otimes \mathbf{n})^S \cdot \mathbf{p} = 0$$

$$
\begin{aligned}
A_{qq} &= \mathbf{q}\cdot\mathbf{A}\cdot\mathbf{q} = \mathbf{q}\cdot(\llbracket\mathbf{u}\rrbracket\otimes\mathbf{n})^{S}\cdot\mathbf{q} = 0 \\
A_{pq} &= \mathbf{p}\cdot\mathbf{A}\cdot\mathbf{q} = \mathbf{p}\cdot(\llbracket\mathbf{u}\rrbracket\otimes\mathbf{n})^{S}\cdot\mathbf{q} = 0
\end{aligned}
\qquad (II.4.1)
$$

$$
\begin{aligned}
A_{nn} &= \mathbf{n}\cdot\mathbf{A}\cdot\mathbf{n} = \mathbf{n}\cdot(\llbracket\mathbf{u}\rrbracket\otimes\mathbf{n})^{S}\cdot\mathbf{n} = \llbracket\mathbf{u}\rrbracket\cdot\mathbf{n} = \llbracket u\rrbracket_n \\
A_{np} &= \mathbf{n}\cdot\mathbf{A}\cdot\mathbf{p} = \mathbf{n}\cdot(\llbracket\mathbf{u}\rrbracket\otimes\mathbf{n})^{S}\cdot\mathbf{p} = \frac{1}{2}\llbracket\mathbf{u}\rrbracket\cdot\mathbf{p} = \frac{1}{2}\llbracket u\rrbracket_p \\
A_{nq} &= \mathbf{n}\cdot\mathbf{A}\cdot\mathbf{q} = \mathbf{n}\cdot(\llbracket\mathbf{u}\rrbracket\otimes\mathbf{n})^{S}\cdot\mathbf{q} = \frac{1}{2}\llbracket\mathbf{u}\rrbracket\cdot\mathbf{q} = \frac{1}{2}\llbracket u\rrbracket_q
\end{aligned}
\qquad (II.4.2)
$$

where $\llbracket u\rrbracket_n$, $\llbracket u\rrbracket_p$ and $\llbracket u\rrbracket_q$ are, respectively, the components of the jump $\llbracket\mathbf{u}\rrbracket$ in $\mathbf{n},\mathbf{p},\mathbf{q}$. So, from eq.(II.4.1) we can write:

$$
\begin{aligned}
\llbracket u\rrbracket_n &= \llbracket\mathbf{u}\rrbracket\cdot\mathbf{n} = A_{nn} \\
\llbracket u\rrbracket_p &= \llbracket\mathbf{u}\rrbracket\cdot\mathbf{p} = 2A_{np} \\
\llbracket u\rrbracket_q &= \llbracket\mathbf{u}\rrbracket\cdot\mathbf{n} = 2A_{nq}
\end{aligned}
\qquad (II.5)
$$

II.1. Resolved jump for the isotropic damage model

From eq.(4.2.7), tensor $\mathbf{A}$ in eq.(II.1) can be identified as:

$$
\mathbf{A} = \frac{g_s}{\mathcal{H}}\,\mathbf{C}^{-1} : \boldsymbol{\sigma}_s = \frac{g_s}{\mathcal{H}}\left[-\frac{\nu}{E}\,tr(\boldsymbol{\sigma}_s)\,\mathbf{1} + \frac{1+\nu}{E}\,\boldsymbol{\sigma}_s\right] \qquad (II.6)
$$

where $tr(\cdot)$ means the trace, $\mathbf{1}$ is the second order unit tensor and the expression of $\mathbf{C}^{-1}$ (the elastic compliance fourth order tensor) in terms of the Poisson's ratio ν and Young modulus E has been considered. From eq.(II.4.1) and eq.(II.6):

$$
\begin{aligned}
A_{pp} &= \mathbf{p}\cdot\mathbf{A}\cdot\mathbf{p} = \frac{g_s}{\mathcal{H}}\,\frac{1}{E}\left[(\sigma_{pp}{}_s - \nu(\sigma_{nn}{}_s + \sigma_{qq}{}_s)\right] = 0 \\
A_{qq} &= \mathbf{q}\cdot\mathbf{A}\cdot\mathbf{q} = \frac{g_s}{\mathcal{H}}\,\frac{1}{E}\left[(\sigma_{qq}{}_s - \nu(\sigma_{nn}{}_s + \sigma_{pp}{}_s)\right] = 0 \\
A_{pq} &= \mathbf{p}\cdot\mathbf{A}\cdot\mathbf{q} = \frac{g_s}{\mathcal{H}}\,\frac{(1+\nu)}{E}\,\sigma_{pq}{}_s = 0
\end{aligned}
\qquad (II.7)
$$

so that eq.(II.7) leads to the following values for the stresses:

$$
\begin{aligned}
\sigma_{pp}{}_s &= \frac{\nu}{1-\nu}\,\sigma_{nn}{}_s \\
\sigma_{qq}{}_s &= \frac{\nu}{1-\nu}\,\sigma_{nn}{}_s \\
\sigma_{pq}{}_s &= 0
\end{aligned}
\qquad (II.8)
$$

Then, from eqs.(II.4.2) and (II.8) one arrives to:

$$
\begin{aligned}
A_{nn} &= \mathbf{n}\cdot\mathbf{A}\cdot\mathbf{n} = \frac{g_s}{\mathcal{H}}\,\frac{1}{E}\left[(\sigma_{nn}{}_s - \nu(\sigma_{pp}{}_s + \sigma_{qq}{}_s)\right] = \\
&\qquad \frac{g_s}{\mathcal{H}}\,\frac{1}{E}\,\frac{(1+\nu)(1-2\nu)}{1-\nu}\,\sigma_{nn}{}_s \\
A_{np} &= \mathbf{n}\cdot\mathbf{A}\cdot\mathbf{p} = \frac{g_s}{\mathcal{H}}\,\frac{1+\nu}{E}\,\sigma_{np}{}_s \\
A_{nq} &= \mathbf{n}\cdot\mathbf{A}\cdot\mathbf{q} = \frac{g_s}{\mathcal{H}}\,\frac{1+\nu}{E}\,\sigma_{nq}{}_s
\end{aligned}
\qquad (II.9)
$$

Finally, from eqs.(II.9) and (II.5) we get:

$$
\begin{bmatrix}\llbracket\mathbf{u}\rrbracket_n \\ \llbracket\mathbf{u}\rrbracket_p \\ \llbracket\mathbf{u}\rrbracket_q\end{bmatrix}_s = \frac{g_s}{\mathcal{H}}\,\frac{1}{E}\begin{bmatrix}\frac{(1+\nu)(1-2\nu)}{1-\nu} & 0 & 0 \\ 0 & 1+\nu & 0 \\ 0 & 0 & 1+\nu\end{bmatrix}\begin{bmatrix}\sigma_{nn} \\ \sigma_{np} \\ \sigma_{nq}\end{bmatrix}_s \qquad (II.10)
$$

II.2. Resolved jump for the plasticity model

From eqs.(5.4.2.) tensor $\mathbf{A}$ of eq.(II.1) can be identified as:

$$\begin{aligned} \mathbf{A} &= \gamma\, \nabla\dot{\phi}_s \\ \gamma &= \frac{1}{\mathcal{H}}\, \dot{\boldsymbol{\sigma}}_s : \nabla\dot{\phi}(\boldsymbol{\sigma}_s) = \frac{1}{\mathcal{H}}\dot{\phi}_s \end{aligned} \tag{II.11}$$

and eqs.(II.4.1), (II.4.2) and (II.5) hold in terms of $[\![\dot{\mathbf{u}}]\!]_s$. Thus, substituting eq.(II.11) into eq.(II.4.1) one obtain:

$$\begin{aligned} A_{pp} &= \mathbf{p}\cdot\mathbf{A}\cdot\mathbf{p} = 0 \Longrightarrow \mathbf{p}\cdot\nabla\dot{\phi}_s\cdot\mathbf{p} = 0 \Longrightarrow \left.\frac{\partial\dot{\phi}(\boldsymbol{\sigma})}{\partial\sigma_{pp}}\right|_s = 0 \\ A_{qq} &= \mathbf{q}\cdot\mathbf{A}\cdot\mathbf{q} = 0 \Longrightarrow \mathbf{q}\cdot\nabla\dot{\phi}_s\cdot\mathbf{q} = 0 \Longrightarrow \left.\frac{\partial\dot{\phi}(\boldsymbol{\sigma})}{\partial\sigma_{qq}}\right|_s = 0 \\ A_{pq} &= \mathbf{p}\cdot\mathbf{A}\cdot\mathbf{q} = 0 \Longrightarrow \mathbf{p}\cdot\nabla\dot{\phi}_s\cdot\mathbf{q} = 0 \Longrightarrow \left.\frac{\partial\dot{\phi}(\boldsymbol{\sigma})}{\partial\sigma_{pq}}\right|_s = 0 \end{aligned} \tag{II.12}$$

and substituting eq.(II.11) into eq.(II.4.2):

$$\begin{aligned} A_{nn} &= \mathbf{n}\cdot\mathbf{A}\cdot\mathbf{n} = \gamma\,\mathbf{n}\cdot\nabla\dot{\phi}_s\cdot\mathbf{n} = \gamma\left.\frac{\partial\dot{\phi}(\boldsymbol{\sigma})}{\partial\sigma_{nn}}\right|_s \\ A_{np} &= \mathbf{n}\cdot\mathbf{A}\cdot\mathbf{p} = \gamma\,\mathbf{n}\cdot\nabla\dot{\phi}_s\cdot\mathbf{p} = \gamma\left.\frac{\partial\dot{\phi}(\boldsymbol{\sigma})}{\partial\sigma_{np}}\right|_s \\ A_{nq} &= \mathbf{n}\cdot\mathbf{A}\cdot\mathbf{q} = \gamma\,\mathbf{n}\cdot\nabla\dot{\phi}_s\cdot\mathbf{q} = \gamma\left.\frac{\partial\dot{\phi}(\boldsymbol{\sigma})}{\partial\sigma_{nq}}\right|_s \end{aligned} \tag{II.13}$$

Then, from eq.(II.13) the components of $[\![\dot{\mathbf{u}}]\!]_s$ can be computed as (see also eqs.(II.5) and (II.11.b)):

$$\begin{aligned} [\![\dot{u}]\!]_{n_s} &= [\![\dot{\mathbf{u}}]\!]_s\cdot\mathbf{n} = A_{nn} = \frac{1}{\mathcal{H}}\,\dot{\phi}_s\left.\frac{\partial\dot{\phi}(\boldsymbol{\sigma})}{\partial\sigma_{nn}}\right|_s \\ [\![\dot{u}]\!]_{p_s} &= [\![\dot{\mathbf{u}}]\!]_s\cdot\mathbf{p} = 2A_{np} = \frac{2}{\mathcal{H}}\,\dot{\phi}_s\left.\frac{\partial\dot{\phi}(\boldsymbol{\sigma})}{\partial\sigma_{np}}\right|_s \\ [\![\dot{u}]\!]_{q_s} &= [\![\dot{\mathbf{u}}]\!]_s\cdot\mathbf{q} = 2A_{nq} = \frac{2}{\mathcal{H}}\,\dot{\phi}_s\left.\frac{\partial\dot{\phi}(\boldsymbol{\sigma})}{\partial\sigma_{nq}}\right|_s \end{aligned} \tag{II.14}$$

where, from eq.(II.12), $\dot{\phi}_s$ can be expressed only in terms of the components of the rate of the traction vector $\dot{\boldsymbol{\sigma}}_s\cdot\mathbf{n} = (\dot{\sigma}_{nn}, \dot{\sigma}_{np}, \dot{\sigma}_{nq})^T_s$ as:

$$\dot{\phi}_s = \left.\frac{\partial\dot{\phi}(\boldsymbol{\sigma})}{\partial\sigma_{nn}}\right|_s \dot{\sigma}_{nn_s} + 2\left.\frac{\partial\dot{\phi}(\boldsymbol{\sigma})}{\partial\sigma_{np}}\right|_s \dot{\sigma}_{np_s} + 2\left.\frac{\partial\dot{\phi}(\boldsymbol{\sigma})}{\partial\sigma_{nq}}\right|_s \dot{\sigma}_{nq_s} \tag{II.15}$$

Eqs.(II.14) and (II.15) provide the resolved (rate of the) displacement jump in terms of the (rate of the) stresses.

II.3. Application to the J_2 flow theory

In the J_2 flow theory case the yield function is defined by:

$$\phi(\boldsymbol{\sigma}) = \sqrt{\frac{3}{2}\left[\boldsymbol{\sigma} : \boldsymbol{\sigma} - \frac{1}{3} tr^2(\boldsymbol{\sigma})\right]} = \sqrt{\frac{3}{2}}\,\|\mathbf{S}\| \tag{II.16}$$

where $\|\cdot\|$ stands for the norm and $\mathbf{S}$ are the deviatoric stresses :

$$\mathbf{S} = \boldsymbol{\sigma} - \frac{1}{3}\, tr(\boldsymbol{\sigma})\, \mathbf{1} \tag{II.17}$$

so that $tr(\mathbf{S}) = 0$. From eqs.(II.16) and (II.17) it is straightforward to check that:

$$\nabla\phi(\boldsymbol{\sigma}) = \sqrt{\frac{3}{2}}\,\frac{\mathbf{S}}{\|\mathbf{S}\|} \tag{II.18}$$

Thus, taking in to account eq.(II.18), for the J_2 flow theory case eq.(II.12) states that: $S_{pp} = S_{qq} = S_{pq} = 0$ and then $tr(\mathbf{S}) = S_{nn} + S_{pp} + S_{qq} = 0 \implies S_{nn} = 0$ so that the deviatoric stress field is reduced to:

$$\mathbf{S}_s = \begin{bmatrix} 0 & \sigma_{np} & \sigma_{nq} \\ \sigma_{np} & 0 & 0 \\ \sigma_{nq} & 0 & 0 \end{bmatrix}_s \tag{II.19}$$

and, thus, from eq.(II.16):

$$\begin{aligned} \dot{\phi}_s &= \sqrt{\frac{3}{2}}\,\|\mathbf{S}_s\| = \sqrt{\frac{3}{2}}\,(\sigma_{np}{}_s^2 + \sigma_{pn}{}_s^2 + \sigma_{nq}{}_s^2 + \sigma_{qn}{}_s^2)^{\frac{1}{2}} \\ &= \sqrt{3}\,(\sigma_{np}{}_s^2 + \sigma_{nq}{}_s^2)^{\frac{1}{2}} \qquad (II.20) \\ \dot{\phi}_s &= \frac{\sqrt{3}}{(\sigma_{np}{}_s^2 + \sigma_{nq}{}_s^2)^{\frac{1}{2}}}\,(\sigma_{np}{}_s\dot{\sigma}_{np}{}_s + \sigma_{nq}{}_s\dot{\sigma}_{nq}{}_s) \qquad (II.21) \end{aligned}$$

Then, substitution of eq.(II.21) into eq.(II.14) taking into account eq.(II.18) leads to:

$$[\![\dot{u}]\!]_{n_s} = 0 \tag{II.22}$$

$$\begin{bmatrix} [\![\dot{u}]\!]_p \\ [\![\dot{u}]\!]_q \end{bmatrix}_s = \frac{3}{\mathcal{H}}\,\frac{1}{\sigma_{np}{}_s^2 + \sigma_{nq}{}_s^2} \begin{bmatrix} \sigma_{np}{}^2 & \sigma_{np}\sigma_{pq} \\ \sigma_{np}\sigma_{nq} & \sigma_{nq}{}^2 \end{bmatrix}_s \begin{bmatrix} \dot{\sigma}_{np} \\ \dot{\sigma}_{nq} \end{bmatrix}_s \tag{II.23}$$

Finally for 2D cases (planes stress-plane strain) where $\mathbf{n}$ and $\mathbf{p}$ define the plane of analysis and σ_{nq_s} is assumed to be zero eqs.(II.22) and (II.23) read:

$$\begin{aligned} [\![\dot{u}]\!]_{n_s} &= 0 \\ \underbrace{[\![\dot{u}]\!]_{p_s}}_{\dot{\gamma}_s} &= \frac{3}{\mathcal{H}}\,\underbrace{\dot{\sigma}_{np_s}}_{\dot{\tau}_s} \implies \dot{\gamma}_s = \frac{3}{\mathcal{H}}\dot{\tau}_s \end{aligned} \tag{II.24}$$

APPENDIX III
ANALYSIS OF THE DISCONTINUITY DIRECTION FOR 2D CASES

III.1. Isotropic damage model

Denoting by $\mathbf{n}$ and $\mathbf{t}$ the unit vectors normal and tangent, respectively, to the discontinuity line S, and considering the orthogonal basis $\hat{\mathbf{e}}_1, \hat{\mathbf{e}}_2$ ($\hat{\mathbf{e}}_1 = \mathbf{n}$, $\hat{\mathbf{e}}_2 = \mathbf{t}$), the equation:

$$\mathbf{t} \cdot \bar{\boldsymbol{\varepsilon}} \cdot \mathbf{t} = \bar{\varepsilon}_{tt} = 0 \qquad (III.1)$$

states that the regular part of the strain $\bar{\boldsymbol{\varepsilon}}$ has a nul term $\bar{\varepsilon}_{tt}$ which, resorting to the Mohrś Circle concepts, is represented in Fig. 5a. From this, different possibilities for the formation of a strong discontinuity emerge: If the principal strains $\bar{\varepsilon}_I$ and $\bar{\varepsilon}_{II}$ are both positive or both negative (see Fig. 5b), eq.(III.1) has no solution for $\mathbf{t}$ and localization is precluded at the considered material point. On the contrary, if $\bar{\varepsilon}_I \cdot \bar{\varepsilon}_{II} < 0$ two possible planes of discontinuity are provided (see Fig. 5c). It is worth noting that a unique solution for the discontinuity direction exists only when one of the principal strains is zero, as can be checked from Fig. 5c.

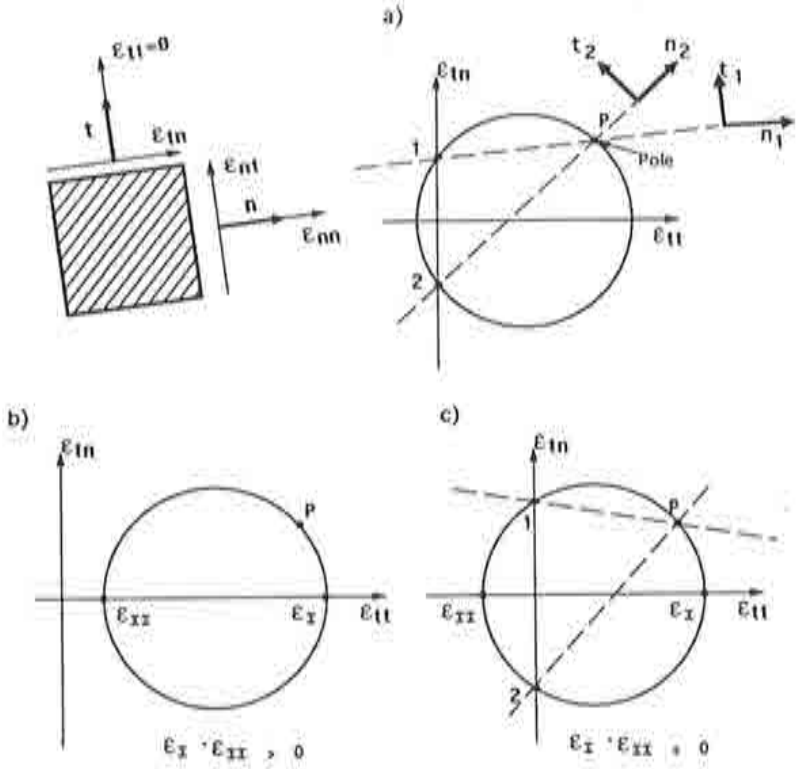

Figure 5. *Computation of the discontinuity direction resorting to the Mohr Circle concepts.*

a) Uniaxial stress for plane stress cases

The imposed uniform stress field reads:

$$\boldsymbol{\sigma} = \begin{bmatrix} \sigma_{11} & \sigma_{12} \\ \sigma_{12} & \sigma_{22} \end{bmatrix} = \begin{bmatrix} \sigma & 0 \\ 0 & 0 \end{bmatrix} \qquad (III.2)$$

and from the isotropic elastic constitutive equation (4.2.6) the regular strain field can be expressed in terms of the Young modulus E and Poisson's ratio ν as:

$$\underline{\varepsilon} = \begin{bmatrix} \varepsilon_{11} & \varepsilon_{12} \\ \varepsilon_{12} & \varepsilon_{22} \end{bmatrix} = \frac{\sigma}{E} \begin{bmatrix} 1 & 0 \\ 0 & -\nu \end{bmatrix} \qquad (III.3)$$

so that from eq.(III.3):

$$\underline{\varepsilon}_I \cdot \underline{\varepsilon}_{II} = -\nu \frac{\sigma^2}{E^2} < 0 \qquad (III.4)$$

Thus, two directions exist which can be identified from eq.(4.4.11) as:

$$tan\,(\theta) = \frac{\pm\sqrt{-\varepsilon_{11}\,\varepsilon_{22}}}{\varepsilon_{11}} = \pm\sqrt{-\frac{\varepsilon_{11}}{\varepsilon_{11}}} = \pm\sqrt{\nu} \qquad (III.5)$$

b) Uniaxial stress for plane strain cases

The stress field is given by eq.(III.2). The strain field is then:

$$\underline{\varepsilon} = \begin{bmatrix} \varepsilon_{11} & \varepsilon_{12} \\ \varepsilon_{12} & \varepsilon_{22} \end{bmatrix} = \frac{\sigma}{E} \begin{bmatrix} 1-\nu^2 & 0 \\ 0 & -\nu(1+\nu) \end{bmatrix} \qquad (III.6)$$

and thus:

$$\underline{\varepsilon}_I \cdot \underline{\varepsilon}_{II} = -\nu(1-\nu^2)(1+\nu)\,\frac{\sigma^2}{E^2} < 0 \qquad (III.7)$$

Finally,

$$tan\,(\theta) = \frac{\pm\sqrt{-\varepsilon_{11}\,\varepsilon_{22}}}{\varepsilon_{11}} = \pm\sqrt{-\frac{\varepsilon_{22}}{\varepsilon_{11}}} = \pm\sqrt{\frac{\nu}{(1-\nu)}} \qquad (III.8)$$

c) Uniaxial strain case

The imposed strain field is:

$$\underline{\varepsilon} = \begin{bmatrix} \varepsilon_{11} & \varepsilon_{12} \\ \varepsilon_{12} & \varepsilon_{22} \end{bmatrix} = \begin{bmatrix} \varepsilon & 0 \\ 0 & 0 \end{bmatrix} \qquad (III.9)$$

thus,

$$\underline{\varepsilon}_I \cdot \underline{\varepsilon}_{II} = 0$$

and:

$$tan\,(\theta) = \pm\sqrt{-\frac{\varepsilon_{22}}{\varepsilon_{11}}} = 0 \qquad (III.10)$$

and only one solution ($\theta = 0$) for the direction of the discontinuity exists.

III.2. J2 Flow Theory

For J2 flow theory cases it can be shown (see Appendix II, section II.3) that the deviatoric stress components in the cartesian axes defined by **n** and **t** are given by:

$$\underline{S} = \begin{bmatrix} S_{nn} & \sigma_{nt} \\ \sigma_{nt} & S_{tt} \end{bmatrix} = \begin{bmatrix} 0 & \tau \\ \tau & 0 \end{bmatrix} \qquad (III.11)$$

so that a *pure shear* deviatoric stress state, appears at the discontinuity line. From eq.(III.11) inmediately emerges that the inclination angle of **n** *with respect to the maximum principal deviatoric stress* is given by:

$$\theta = \pm\frac{\pi}{4} \qquad (III.12)$$

Since the principal directions of the stress and the deviatoric stress tensors are tha same, eq. (III.12) also holds for the complete stress tensor.

PART II:

NUMERICAL SIMULATION

SUMMARY

On the basis of the strong discontinuity analysis of standard local stress-strain constitutive equations, a finite element framework for the simulation of strong discontinuities, which can be inscribed in the family of assumed enhanced strain methods, is presented. Taking the standard linear triangle as underlying element, an additional incompatible mode leads to the formulation of an enriched strain field which is shown to be able to appropriately capture strong discontinuities. The presented numerical simulations show that mesh size and mesh alignment dependencies can be completely removed.

1. INTRODUCTION

In Part I of this work the so called *strong discontinuity analysis* (S.D.A) was introduced. As shown there, the application of the S.D.A to any standard (local, stress-vs-strain) constitutive equation provides a general framework in which the analysis and simulation of the strong discontinuity problem could be inscribed. In particular some key conditions for these constitutive equations are derived (the distributional character of the softening parameter is the most relevant one) which, together with some additional requirements, provide a well posed set of partial differential equations governing the strong discontinuity problem.

In this (second) part of the work, the finite element approximation to the solution of the strong discontinuity problem is addressed. At this point it should be emphasized that the solution of the problem lies in the space of *discontinuous* displacements and, consequently, *unbounded* strains. Regarding the numerical simulation of the problem, this fact suggests that standard $\mathcal{C}^0$ finite element approximations to the displacement field would have to find intrinsic difficulties when applied to the strong discontinuity problem.

In fact, the well known mesh alignment dependencies appearing in classical smeared or *continuum* approaches[10,16] could be regarded as consequence of these difficulties. Therefore, derivation and use of finite element approaches including discontinuous displacement fields, could be envisaged as a suitable remedy for the aforementioned problems[3,4,5,9,11,18,19].

In this work a finite element formulation is presented, in which the incorporation of the additional discontinuous displacement field to the standard finite element approach is done in the framework of the *assumed enhanced strain* (A.E.S) methods[17] that is to say: an appropriate incompatible mode containing an approximation to the displacement jump is added to the underlying standard C^0 element. Previous attempts to resort to A.E.S methods in finite element localization analysis can be found, for example, in references [1,13,20]. The introduction of discontinuous displacement fields has the drawback of dealing with strain fields containing Dirac delta-functions which, in this work, are approximated by regularized (bounded) delta-sequences in terms of a regularization parameter. This procedure allows to escape from the inherent difficulties of dealing with unbounded functions in the numerical approach. On this basis, a resulting formulation has been derived for 2D cases taking the three noded linear triangle as underlying element. Its reliability is checked by resorting to different basic tests and the simulation of several strong discontinuity problems.

2. FIELD EQUATIONS

Let us consider the reference configuration of the body Ω with boundary $\partial\Omega$. Let $\Gamma_u \subset \partial\Omega$ and $\Gamma_\sigma \subset \partial\Omega$ ($\Gamma_u \cup \Gamma_\sigma = \partial\Omega$, $\Gamma_u \cap \Gamma_\sigma = \emptyset$) be the boundaries subjected to the usual essential and natural conditions, respectively. Let finally $\mathcal{S}$ be the discontinuity (material) surface splitting the body into two parts Ω^+ and Ω^-, $\mathbf{n}$ the unit vector normal to $\mathcal{S}$ (pointing to Ω^+) and $\boldsymbol{\nu}$ the outward normal to the external boundary $\partial\Omega$ (see Fig. 1).

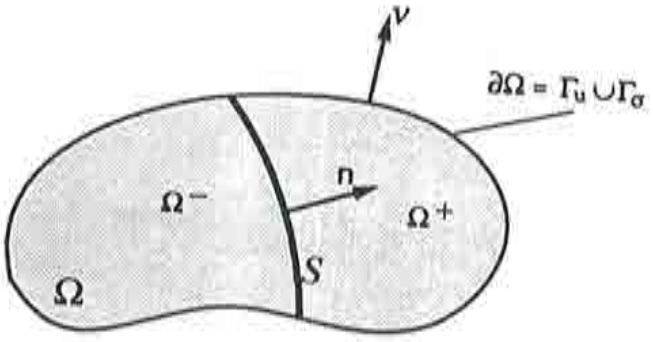

Figure 1. *Definition of the discontinuity path.*

The field equations governing the boundary value problem can be written as:

$$\nabla \cdot \boldsymbol{\sigma} + \mathbf{f} = \mathbf{0} \qquad in \qquad \Omega \backslash \mathcal{S} \tag{2.1}$$

$$\mathbf{u} = \mathbf{u}^* \quad in \quad \Gamma_u \tag{2.2}$$

$$\boldsymbol{\sigma} \cdot \boldsymbol{\nu} = \mathbf{t}^* \quad in \quad \Gamma_\sigma \tag{2.3}$$

$$\boldsymbol{\sigma}^+ \cdot \mathbf{n} = \boldsymbol{\sigma}^- \cdot \mathbf{n} \quad in \quad \mathcal{S} \tag{2.4}$$

$$\boldsymbol{\sigma}_s \cdot \mathbf{n} = \boldsymbol{\sigma}^+ \cdot \mathbf{n} \ \ (= \boldsymbol{\sigma}^- \cdot \mathbf{n}) \quad in \quad \mathcal{S} \tag{2.5}$$

Eq. (2.1), where $\boldsymbol{\sigma}$ are the stresses and $\mathbf{f}$ corresponds to the body forces, is the classical equilibrium equation for the quasistatic problem. Eqs.(2.2) and (2.3) state the essential an natural boundary conditions, respectively ($\mathbf{u}$ corresponds to the displacement field and $\mathbf{u}^*$ and $\mathbf{t}^*$ are the prescribed displacement and traction vectors, respectively). Eqs. (2.4) and (2.5) state the continuity of the traction vector across the discontinuity surface $\mathcal{S}$. In particular, eq.(2.4), where $\boldsymbol{\sigma}^+$ and $\boldsymbol{\sigma}^-$ stand for the stress fields in Ω^+ and Ω^-, respectively, involves the traction vectors ($\boldsymbol{\sigma}^+ \cdot \mathbf{n}$ and $\boldsymbol{\sigma}^- \cdot \mathbf{n}$) at *both* sides of $\mathcal{S}$ whereas in eq.(2.5), where $\boldsymbol{\sigma}_s$ stands for the stress field in $\mathcal{S}$, the traction vector *at* the discontinuity surface ($\boldsymbol{\sigma}_s \cdot \mathbf{n}$) is also involved. Eqs.(2.1) to (2.3) are field equations for classical problems, eq.(2.4) is included when considering *weak* discontinuities[6] whereas eq.(2.5) is specific for problems exhibiting *strong* discontinuities.

The previous set of equations is complemented by the *constitutive equations*, defining the stresses in terms of the strains, and the *kinematic equations* defining the strains in terms of the displacement field. Constitutive and kinematic equations have been studied in depth in Part I of this work. As a consequence of the so called strong discontinuity analysis, performed there on two different families of constitutive equations (isotropic continuum damage and elasto-plasticity), the softening parameter must be reinterpreted in a distributional sense: the inverse of the softening parameter $\mathcal{H}$ has the structure of a delta-function defined on $\mathcal{S}$, i.e.:

$$\frac{1}{\mathcal{H}} = \delta_s \frac{1}{\bar{\mathcal{H}}} \tag{2.6}$$

where $\bar{\mathcal{H}} < 0$ is the so called *intrinsic softening parameter* which can be interpreted as a material property defined in terms of the *fracture energy* (see Part I[12], sections 4.5 and 5.5), and δ_s is a delta-function along $\mathcal{S}$. Eq.(2.6) states the elastic behaviour outside $\mathcal{S}$ ($\frac{1}{\mathcal{H}} = 0 \Longrightarrow \mathcal{H} = \infty \Longrightarrow$ *elastic behaviour*) and leads, for the different standard constitutive equations, to the derivation of stress-jump relationships as their consistent *discrete* counterpart in $\mathcal{S}$ (see Part I[12], sections 4.2 and 5.2). However there is no need, in the actual analysis, to directly resort to those discrete constitutive equations which are implicitly fulfilled by imposing condition (2.6) in the standard constitutive equations. So, standard non-linear stress-strain constitutive equations of the type:

$$\boldsymbol{\sigma} = \boldsymbol{\sigma}(\boldsymbol{\epsilon}) \tag{2.7}$$

allowing for strain-softening mechanisms governed by eq.(2.6) can be considered in the analysis.

Concerning to the kinematic equations, consideration of the appearance of strong discontinuities leads to the definition of the strain field not only in terms of the regular part of the displacement $\bar{\mathbf{u}}$, but also in terms of the displacement jump $[\![\mathbf{u}]\!]_s$ and the normal $\mathbf{n}$ (see Part I[12], section 2), so that:

$$\boldsymbol{\epsilon} = \boldsymbol{\epsilon}\,(\bar{\mathbf{u}}, [\![\mathbf{u}]\!]_s, \mathbf{n}) \tag{2.8}$$

In eq.(2.8) $[\![\mathbf{u}]\!]_S$ and $\mathbf{n}$ are additional unknowns with respect to the standard solid mechanics problem. The normal $\mathbf{n}$, at any point of $\mathcal{S}$, can be computed in terms of the stress field at the initiation time (see Part I[12], sections 4.5 and 5.4) so that, finally, only the jump $[\![\mathbf{u}]\!]_S$ remains as the additional unknown. Finally, the traction vector continuity condition (2.5) provides the required additional set of equations to solve for the jump.

In summary, the field equations (2.1) to (2.5) supplemented by the standard constitutive equation (2.7) (with distributional softening) and the kinematic equation (2.8) provide a sufficient and well posed set of equations to solve the boundary value problem in terms of $\boldsymbol{\sigma}$, $\boldsymbol{\epsilon}$, $\bar{\mathbf{u}}$ and $[\![\mathbf{u}]\!]_S$.

3. REFORMULATION OF THE KINEMATICS: THE ESSENTIAL BOUNDARY CONDITIONS

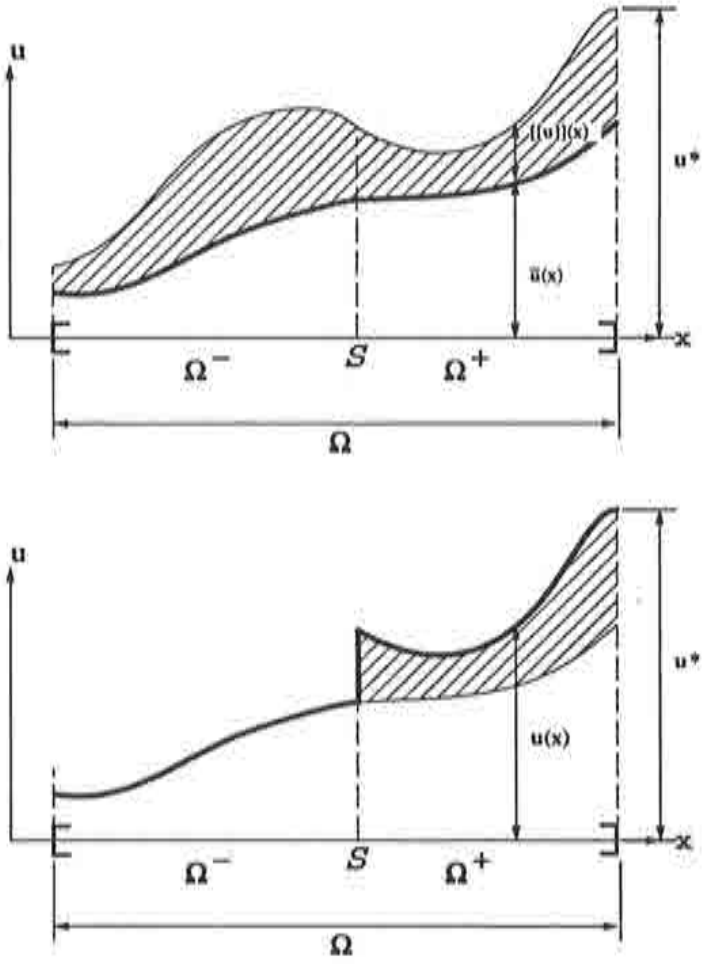

Figure 2. *Kinematics: A possible decomposition of the displacement field.*

For the sake of simplicity in Part I of this work the displacement field in

presence of strong discontinuities was written as (see Part I[12], section 2):

$$\mathbf{u}(\mathbf{x},\, t) = \bar{\mathbf{u}}(\mathbf{x},\, t) + H_{\mathcal{S}}\,(\mathbf{x})[\![\mathbf{u}]\!](\mathbf{x},\, t) \tag{3.1}$$

where $\mathbf{u}(\mathbf{x},\, t)$ stands for the regular (continuous) displacement field, $H_{\mathcal{S}}\,(\mathbf{x})$ is the Heaviside function on $\mathcal{S}$ ($H = 0$ on Ω^- and $H = 1$ on Ω^+) and $[\![\mathbf{u}]\!](\mathbf{x},\, t)$ is a displacement jump function. In Fig. 2 an schematic illustration of eq.(3.1) for 1D cases is depicted.

Imposition of the essential boundary conditions (2.2) can not be done on just *one* of the fields $\bar{\mathbf{u}}$ or $[\![\mathbf{u}]\!]$ as can be checked in Fig. 2. In order to overcome this difficulty a different kinematic decomposition can be devised as follows:

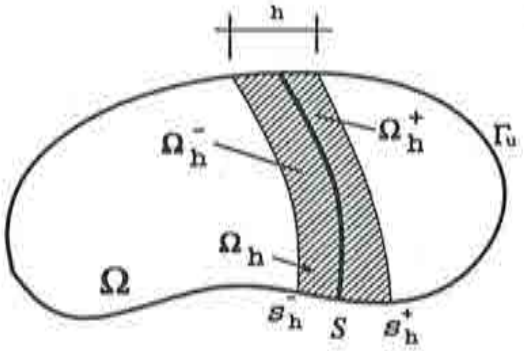

Figure 3. *Definition of the domain* Ω^h.

Let us consider an additional subdomain $\Omega^h \subset \Omega$ surrounding $\mathcal{S}$ ($\mathcal{S} \subset \Omega^h$ see Fig. 3), defined by two arbitrary boundaries *ahead* ($\mathcal{S}_h^+$) and *behind* ($\mathcal{S}_h^-$) the discontinuity surface, and splitted by $\mathcal{S}$ into the subdomains Ω_h^+ and Ω_h^-. It is assumed that the boundary Γ_u, where the essential boundary conditions are imposed, is outside Ω^h ($\Gamma_u \cap \Omega^h = \emptyset$). Then, we can define a continuous function $\varphi^h(\mathbf{x})$ which is completely arbitrary except for the following two conditions:

$$\begin{aligned} \varphi^h(\mathbf{x}) &= 0 \quad \forall \mathbf{x} \in \Omega^- \backslash \Omega_h^- \\ \varphi^h(\mathbf{x}) &= 1 \quad \forall \mathbf{x} \in \Omega^+ \backslash \Omega_h^+ \end{aligned} \tag{3.2}$$

Let us now consider the function $\mathcal{M}_{\mathcal{S}}^h(\mathbf{x})$ defined as:

$$\mathcal{M}_{\mathcal{S}}^h(\mathbf{x}) = H_{\mathcal{S}}(\mathbf{x}) - \varphi^h(\mathbf{x}) \tag{3.3}$$

It is straightforward to check that $\mathcal{M}_{\mathcal{S}}^h(\mathbf{x})$ takes the value zero everywhere in Ω except in Ω_h (the support of $\mathcal{M}_{\mathcal{S}}^h$, see Fig.4 for 1D cases). With these definitions in mind we can now define the continuous function $\hat{\mathbf{u}}(\mathbf{x}, t)$ as:

$$\hat{\mathbf{u}}(\mathbf{x}, t) = \bar{\mathbf{u}}(\mathbf{x}, t) + \varphi^h(\mathbf{x})\, [\![\mathbf{u}]\!](\mathbf{x},\, t) \tag{3.4}$$

and substituting eq.(3.4) into eq.(3.1) we arrive, in view of eq.(3.3), to:

$$\begin{aligned} \mathbf{u}(\mathbf{x}, t) &= \hat{\mathbf{u}}(\mathbf{x}, t) + \left[H_{\mathcal{S}}(\mathbf{x}) - \varphi^h(\mathbf{x})\right] [\![\mathbf{u}]\!](\mathbf{x},\, t) \\ &= \hat{\mathbf{u}}(\mathbf{x}, t) + \mathcal{M}_{\mathcal{S}}^h(\mathbf{x})\, [\![\mathbf{u}]\!](\mathbf{x},\, t) \end{aligned} \tag{3.5}$$

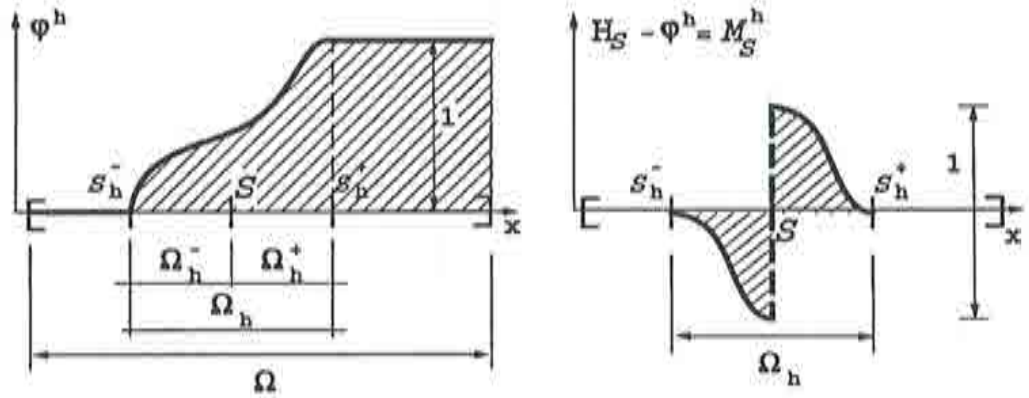

Figure 4. *Construction of the unit jump function.*

Hence, the kinematic description of the displacement field is made now, according to eq.(3.5), in terms of the regular (continuous) part $\hat{\mathbf{u}}(\mathbf{x},t)$ plus the term $\mathcal{M}_s^h[\![\mathbf{u}]\!](\mathbf{x},\ t)$ *which contains the jump and whose support is* Ω_h (see Fig. 5). Thus, the essential boundary conditions can be applied *exclusively* on the term $\hat{\mathbf{u}}(\mathbf{x},t)$. This fact makes the kinematic description (3.5) suitable for numerical computations as will be shown in section 5.

REMARK (3.1)
The kinematic description of eq.(3.5) is completely general. The subdomain Ω_h *is arbitrary in shape and size. Function* φ^h *is completely arbitrary in* Ω_h *with the only requirements of being continuous and the restrictions given in eq.(3.2)*

REMARK (3.2)
The displacement fields given by eqs.(3.1) and (3.5) are completely equivalent. One can pass from one description to the other by using eqs.(3.3) and (3.4). Thus, the different qualitative conclusions emerging from the strong discontinuity analysis performed in Part 1 are fully applicable when eqs.(3.5) are used as the kinematic description, as will be done in next sections.

4. WEAK FORMULATION

Let us consider the virtual work principle stating:

$$\int_\Omega \boldsymbol{\sigma} : \nabla\hat{\boldsymbol{\eta}}\, d\Omega \;=\; \int_\Omega \mathbf{f}\cdot\hat{\boldsymbol{\eta}}\, d\Omega + \int_{\Gamma_\sigma} \mathbf{t}^*\cdot\hat{\boldsymbol{\eta}}\, d\Gamma \tag{4.1}$$

for all the admissible test functions $\hat{\boldsymbol{\eta}} \in \hat{\mathcal{V}}$, where $\hat{\mathcal{V}}$ is the space of the kinematically admissible variations defined by:

$$\hat{\mathcal{V}} := \left\{\hat{\boldsymbol{\eta}} \in C^0 \quad \hat{\boldsymbol{\eta}}\Big|_{\Gamma_u} = 0\right\} \tag{4.2}$$

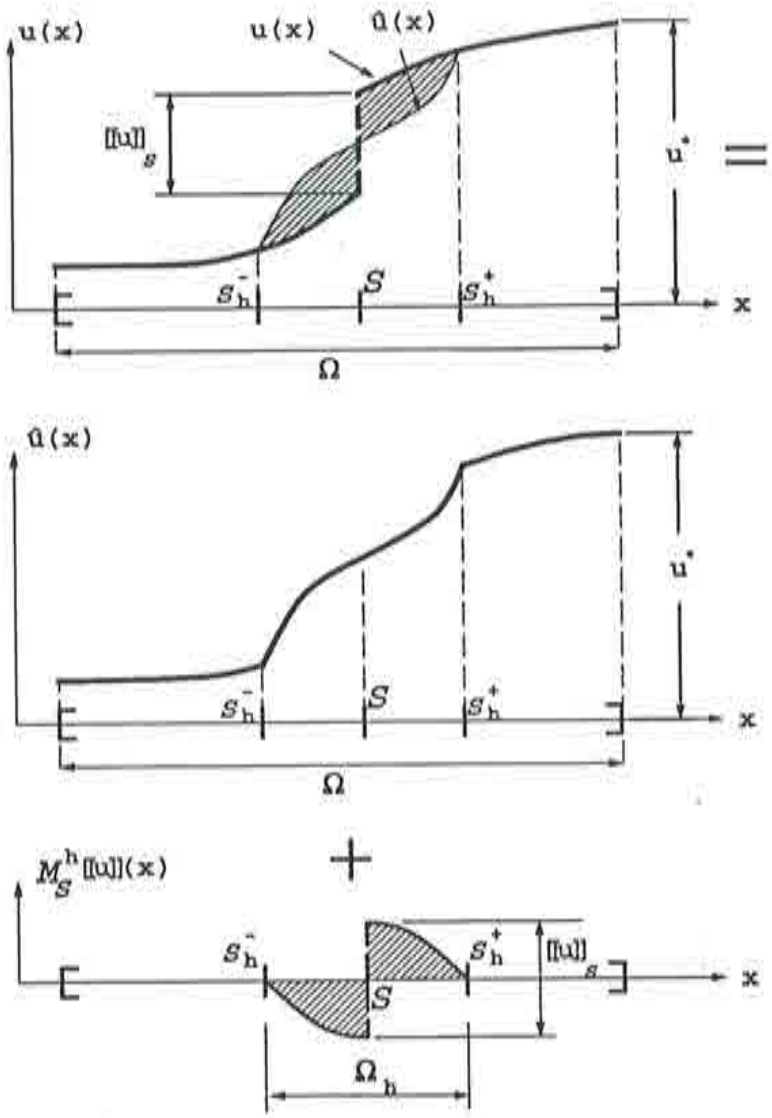

Figure 5. *Kinematics: Suitable decomposition of the displacement field.*

Integration by parts of eq.(4.1), taking into account eq.(4.2), leads to:

$$
\begin{aligned}
\int_{\Omega} \boldsymbol{\sigma} : \nabla \dot{\boldsymbol{\eta}} \, d\Omega \; &= \; \int_{\Omega \setminus \mathcal{S}} \boldsymbol{\sigma} : \nabla \dot{\boldsymbol{\eta}} \, d\Omega \\
= \; - \int_{\Omega \setminus \mathcal{S}} \nabla \boldsymbol{\sigma} \cdot \dot{\boldsymbol{\eta}} \, d\Omega \; &+ \; \int_{\partial\Omega^+ \cup \partial\Omega^-} \boldsymbol{\nu} \cdot \boldsymbol{\sigma} \cdot \dot{\boldsymbol{\eta}} \, d\Gamma \qquad (4.3) \\
= \; - \int_{\Omega \setminus \mathcal{S}} \nabla \boldsymbol{\sigma} \cdot \dot{\boldsymbol{\eta}} \, d\Omega \; &+ \; \int_{\Gamma_\sigma} \boldsymbol{\nu} \cdot \boldsymbol{\sigma} \cdot \dot{\boldsymbol{\eta}} \, d\Gamma - \int_{\mathcal{S}} \mathbf{n} \cdot (\boldsymbol{\sigma}^+ - \boldsymbol{\sigma}^-) \cdot \dot{\boldsymbol{\eta}} \, d\Gamma
\end{aligned}
$$

Inserting eq.(4.3) into eq.(4.1) we arrive finally to:

$$\begin{aligned} &-\int_{\Omega\setminus\mathcal{S}} (\nabla\cdot\boldsymbol{\sigma}+\mathbf{f})\cdot\dot{\boldsymbol{\eta}}\, d\Omega \\ &-\int_{\mathcal{S}} \mathbf{n}\cdot(\boldsymbol{\sigma}^{+}-\boldsymbol{\sigma}^{-})\cdot\dot{\boldsymbol{\eta}}\, d\Gamma+\int_{\Gamma_\sigma}(\boldsymbol{\nu}\cdot\boldsymbol{\sigma}-\mathbf{t}^{*})\cdot\dot{\boldsymbol{\eta}}\, d\Gamma \;=\; 0 \end{aligned} \tag{4.4}$$

Finally, from eqs.(4.4) standard arguments lead to:

$$\begin{aligned} \nabla\cdot\boldsymbol{\sigma}+\mathbf{f} &= \mathbf{0} \quad in \quad \Omega\setminus\mathcal{S} \\ \boldsymbol{\sigma}\cdot\boldsymbol{\nu} &= \mathbf{t}^{*} \quad in \quad \Gamma_\sigma \\ \boldsymbol{\sigma}^{+}\cdot\mathbf{n} &= \boldsymbol{\sigma}^{-}\cdot\mathbf{n} \quad in \quad \mathcal{S} \end{aligned} \tag{4.5}$$

REMARK (4.1)
Comparing eqs.(4.5) with the field equations (2.1) to (2.5) we realize that from the variational principle (4.1), eqs.(2.1), (2.3) and (2.4) are satisfied in weak form. Therefore, besides the standard essential boundary conditions (2.2) only the traction vector continuity condition (2.5) has to be locally imposed on the discontinuity surface $\mathcal{S}$.

5. FINITE ELEMENT APPROXIMATION

For the sake of simplicity we will restrict in the following to 2D cases, although the extension to 3D cases follows quite naturally.

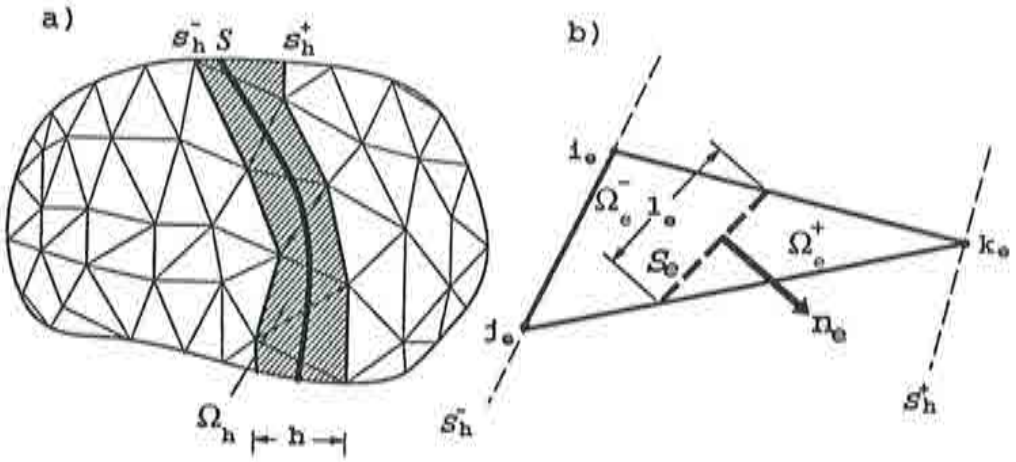

Figure 6. *Finite element approximation to the strong discontinuity problem.*

Let us consider a finite element discretization of Ω based on linear triangular elements as shown in Fig. 6.a. By the time being let us assume the position of $\mathcal{S}$ known (its precise determination will be tackled in section 6). Let us consider the band of finite elements crossed by $\mathcal{S}$ defining the subdomain Ω_h and then the

lines $\mathcal{S}_h^+$ and $\mathcal{S}_h^-$ which are constituted by the sides of the elements belonging to Ω_h and placed ahead of and behind of $\mathcal{S}$, respectively. Let $\mathcal{J}$ denote the set of numbers associated with elements belonging to Ω_h, i.e.:

$$\mathcal{J} := \left\{ e \in 1, 2, ..., E \quad | \quad \Omega_e \subset \Omega_h \right\} \tag{5.1}$$

Each element $e \in \mathcal{J}$ has a side ($\mathcal{S}_{h_e}^-$, defined by the nodes i_e and j_e, see Fig. 6b) belonging to $\mathcal{S}_h^-$ (or to $\mathcal{S}_h^+$) and a node k_e (from now on termed the *solitary node*) belonging to $\mathcal{S}_h^+$ (or to $\mathcal{S}_h^-$). Let $\mathcal{S}_e$ be the straight segment approaching $\mathcal{S}$ inside the element and $\mathbf{n}_e$ the normal to $\mathcal{S}_e$ (assumed to point to k_e). Definition of $\mathcal{S}_e$ and $\mathbf{n}_e$ allows for the determination of subdomains Ω_e^+ and Ω_e^- as indicated in Fig. 6b.

5.1. Displacement and strain fields

Motivated by the kinematic description of eq.(3.5) we assume the following approximation to the displacement field:

$$\mathbf{u}^h(\mathbf{x},t) = \underbrace{\mathbf{N}(\mathbf{x}) \cdot \mathbf{a}(t)}_{\bar{\mathbf{u}}^h(\mathbf{x},t)} + \sum_{e \in \mathcal{J}} \mathcal{M}_{\mathcal{S}_e}^h(\mathbf{x}) \underbrace{\boldsymbol{\alpha}_e(t)}_{[\mathbf{u}]^h(t)} \tag{5.1.1}$$

$$\mathcal{M}_{\mathcal{S}_e}^h(\mathbf{x}) = H_{\mathcal{S}_e}(\mathbf{x}) - \varphi_e^h(\mathbf{x}) \tag{5.1.2}$$

$$\varphi_e^h(\mathbf{x}) = N_{k_e}(\mathbf{x}) \tag{5.1.3}$$

where $\mathbf{N}(\mathbf{x})$ is the standard shape function matrix[21], $\mathbf{a}(t)$ is the nodal displacement vector, $H_{\mathcal{S}_e}(\mathbf{x})$ is the Heaviside function restricted to the domain Ω_e and $N_{k_e}(\mathbf{x})$ is the standard linear shape function corresponding to the *solitary node* k_e. The function $\mathcal{M}_{\mathcal{S}_e}^h(\mathbf{x})$ defined in eq.(5.1.2) is depicted in Fig. 7.

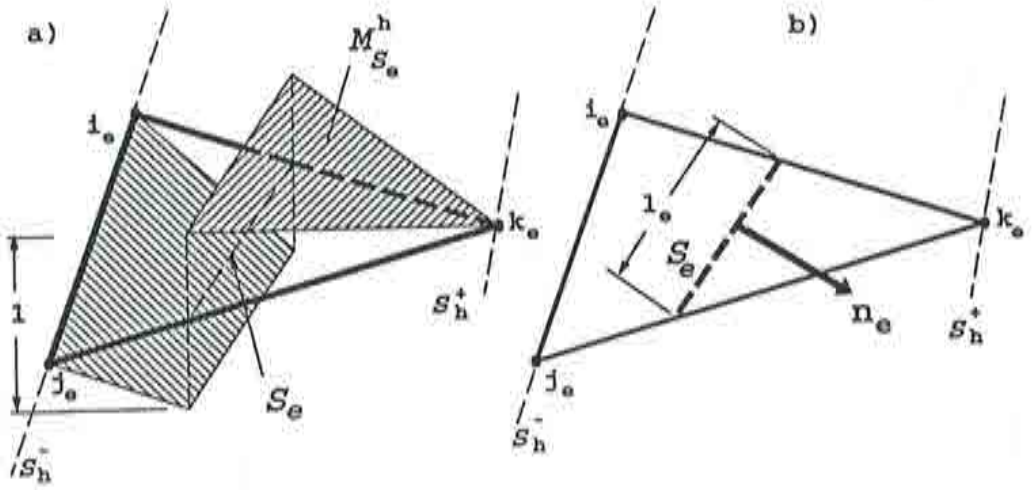

Figure 7. *Finite element approximation to the unit jump function.*

The definition of the displacement field (5.1.1) motivates the following comments:

a) The term $\mathbf{N}(\mathbf{x}) \cdot \mathbf{a}(t)$ in eq.(5.1.1) matches the regular (smooth) part $\hat{\mathbf{u}}(\mathbf{x}, t)$ of the displacement field of eq.(3.5). Thus, as it was stated in section 3, the essential boundary conditions have to be imposed on the corresponding nodal values $\mathbf{a}(t)$ like in the standard finite element approximations.

b) If $\mathcal{M}^h_{\mathcal{S}_e}(\mathbf{x})$ is defined only for the elements belonging to Ω_h, as states eq.(5.1.1), then the displacement field $\mathbf{u}^h(\mathbf{x}, t)$ matches the kinematic description (3.5): the jump function $[\![\mathbf{u}]\!]^h(\mathbf{x}, t)$ is considered piece-wise constant (over the elements) and $\boldsymbol{\alpha}_e(t)$ *plays the role of the displacement jump corresponding to the element* e.

c) If $\mathcal{M}^h_{\mathcal{S}_e}(\mathbf{x})$ is defined *for all the elements of* Ω, then the displacement field $\mathbf{u}^h(\mathbf{x}, t)$ matches the kinematic description (3.5) *provided the jump* $\boldsymbol{\alpha}_e(t)$ *is zero for all the elements of* $\Omega \backslash \Omega^h$. This approach is the one considered in the rest of the analysis so that eq.(5.1.1) has to be slightly modified as follows:

$$\mathbf{u}^h(\mathbf{x}, t) = \underbrace{\mathbf{N}(\mathbf{x}) \cdot \mathbf{a}(t)}_{\hat{\mathbf{u}}^h(\mathbf{x},t)} + \sum_{e=1}^{n_{el}} \mathcal{M}^h_{\mathcal{S}_e}(\mathbf{x})\, \boldsymbol{\alpha}_e(t) \tag{5.1.4}$$

$$\boldsymbol{\alpha}_e(t) = \mathbf{0} \quad \forall e \notin \mathcal{J} \tag{5.1.5}$$

where n_{el} is the total number of elements of the finite element mesh.

From eq.(5.1.4) the strain field is computed as the local (at elemental level) gradient of the displacement field:

$$\boldsymbol{\epsilon}^h(\mathbf{x}, t) = \underbrace{\left(\nabla \hat{\mathbf{u}}^h\right)^S}_{regular \quad \hat{\boldsymbol{\epsilon}}^h} + \underbrace{\sum_{e=1}^{n_{el}} \left(\nabla \mathcal{M}^h_{\mathcal{S}_e} \otimes \boldsymbol{\alpha}_e\right)^S}_{enhanced \quad \tilde{\boldsymbol{\epsilon}}^h} \tag{5.1.6}$$

where $(\cdot)^S$ means the symmetric part of $(\cdot)$. From eqs.(5.1.2) and (5.1.3) we can write:

$$\nabla \mathcal{M}^h_{\mathcal{S}_e} = \begin{cases} \delta_{\mathcal{S}_e} \mathbf{n}_e - \nabla N_{k_e} & \forall \mathbf{x} \in \Omega_e \\ \mathbf{0} & otherwise \end{cases} \tag{5.1.7}$$

where $\delta_{\mathcal{S}_e}$ is the Dirac's delta-function, placed along $\mathcal{S}_e$ and restricted to the domain Ω_e, satisfying:

$$\int_{\Omega_e} \delta_{\mathcal{S}_e}\, \varphi_0\, d\Omega = \int_{\mathcal{S}_e} \varphi_0\, d\Gamma \qquad \forall\, \varphi_0 \in C_0^\infty(\Omega_e) \tag{5.1.8}$$

REMARK (5.1.1)

The displacement and strain fields defined in eqs.(5.1.4) and (5.1.6) inscribe the proposed approach in the so called method of the incompatible modes and, thus, in the family of the assumed enhanced strain (A.E.S) methods[17]. *The term* $\mathcal{M}^h_{\Omega_e}\boldsymbol{\alpha}_e$ *in eq.(5.1.4) can be interpreted as the incompatible mode, corresponding to the element* e, *supplementing the smooth displacement field* $\hat{\mathbf{u}}^h(\mathbf{x},t)$. *In eq.(5.1.6) the term* $(\boldsymbol{\nabla}\mathcal{M}^h_{\Omega_e}\otimes\boldsymbol{\alpha}_e)^S$ *can be understood as the enhanced strain* $\tilde{\boldsymbol{\epsilon}}^h_e$, *piece-wise defined on each element* e, *enriching the regular strain field* $\hat{\boldsymbol{\epsilon}} = (\boldsymbol{\nabla}\hat{\mathbf{u}}^h)^S$.

When dealing, as it is usual for engineering purposes, with the strain ($\boldsymbol{\epsilon} = \{\epsilon_{xx}, \epsilon_{yy}, \gamma_{xy}\}$) and the stress ($\boldsymbol{\sigma} = \{\sigma_{xx}, \sigma_{yy}, \tau_{xy}\}$) vectors ‡ instead of the symmetric strain and stress tensors, the strain field (5.1.6) can be reformulated from eqs.(5.1.4), (5.1.6) and (5.1.7) in a cartesian (x,y) system of coordinates as:

$$\boldsymbol{\epsilon}^h = \hat{\boldsymbol{\epsilon}}^h + \sum_{e=1}^{n_{el}} \tilde{\boldsymbol{\epsilon}}^h_e \tag{5.1.9}$$

$$\hat{\boldsymbol{\epsilon}}^h = \mathbf{B}\cdot\mathbf{a} \tag{5.1.10}$$

$$\tilde{\boldsymbol{\epsilon}}^h_e = \mathbf{G}_e\cdot\boldsymbol{\alpha}_e \tag{5.1.11}$$

$$\mathbf{G}_e(\mathbf{x}) = \begin{cases} \begin{bmatrix} \delta_{\Omega_e} n_x - \frac{\partial N_{h_e}}{\partial x} & 0 \\ 0 & \delta_{\Omega_e} n_y - \frac{\partial N_{h_e}}{\partial y} \\ \delta_{\Omega_e} n_y - \frac{\partial N_{h_e}}{\partial y} & \delta_{\Omega_e} n_x - \frac{\partial N_{h_e}}{\partial x} \end{bmatrix} & \forall \mathbf{x}\in\Omega_e \\ \mathbf{0} & \textit{otherwise} \end{cases} \tag{5.1.12}$$

where $\mathbf{B}$ is the standard deformation matrix[21] and n_x and n_y are the components of $\mathbf{n}_e$ ($\mathbf{n}_e = \{n_x, n_y\}$).

5.2. Discretized set of equations

We now consider the finite element approximation to the weighting space $\hat{\mathcal{V}}$ of eq.(4.2) given by:

$$\hat{\mathcal{V}}^h := \left\{ \hat{\boldsymbol{\eta}}^h \;\middle|\; \hat{\boldsymbol{\eta}}^h = \mathbf{N}\cdot\mathbf{a} \quad \hat{\boldsymbol{\eta}}^h\Big|_{\Gamma_u} = 0 \right\} \tag{5.2.1}$$

Substitution of eq.(5.2.1) into (4.1) leads, through standard arguments, to the following set of equations:

$$\int_\Omega \mathbf{B}^T : \boldsymbol{\sigma}^h d\Omega = \mathbf{f}_{ext} \tag{5.2.2}$$

$$\mathbf{f}_{ext} = \int_\Omega \mathbf{N}^T\cdot\mathbf{f}\, d\Omega + \int_{\Gamma_\sigma} \mathbf{N}^T\cdot\mathbf{t}^*\, d\Gamma \tag{5.2.3}$$

‡ this notation will be used from now on.

where superscript $(\cdot)^T$ means transposition of $(\cdot)$.

REMARK (5.2.1)
Eqs.(5.2.2) are the discrete counterpart of the weak form eq.(4.1). Due to the bounded nature of both the stress field $\boldsymbol{\sigma}^h$ and the deformation matrix $\mathbf{B}$, and since $\mathcal{S}$ has zero measure, the domain of integration Ω of eqs.(5.2.2) could be, if convenient, restricted to $\Omega \backslash \mathcal{S}$ and, therefore, eq.(5.2.2) can be rewritten as:

$$\int_{\Omega} \mathbf{B}^T : \boldsymbol{\sigma}^h d\Omega = \int_{\Omega \backslash \mathcal{S}} \mathbf{B}^T : \boldsymbol{\sigma}^h d\Omega = \mathbf{f}_{ext} \tag{5.2.4}$$

As stated in section 4 (remark 4.1), the set of equations (5.2.4) has to be complemented by the local enforcement of the traction vector continuity condition. Then, eq.(2.5) can be rewritten in terms of the stress vectors as:

$$\boldsymbol{\sigma}_{\mathcal{S}} \cdot \boldsymbol{\mathcal{N}} = \boldsymbol{\sigma}^+ \cdot \boldsymbol{\mathcal{N}} \; (= \boldsymbol{\sigma}^- \cdot \boldsymbol{\mathcal{N}}) = \boldsymbol{\sigma}_{\Omega \backslash \mathcal{S}} \cdot \boldsymbol{\mathcal{N}} \qquad in \; \mathcal{S} \tag{5.2.5}$$

where

$$\boldsymbol{\mathcal{N}} = \begin{bmatrix} n_x & 0 \\ 0 & n_y \\ n_y & n_x \end{bmatrix} \tag{5.2.6}$$

and $\boldsymbol{\sigma}_{\Omega \backslash \mathcal{S}}$ stands for the stresses at $\Omega \backslash \mathcal{S}$.

In the context of the finite element approximation described above, let us consider the following set of equations:

$$\int_{\Omega_e} \mathbf{G}_e^{*T} \cdot \boldsymbol{\sigma}^h \; d\Omega_e = 0 \qquad e = 1 \ldots n_{el} \tag{5.2.7}$$

$$\mathbf{G}_e^* = \begin{cases} (\delta_{\mathcal{S}_e} - \dfrac{l_e}{\Omega_e}) \, \boldsymbol{\mathcal{N}} & \mathbf{x} \in \Omega_e \\ 0 & otherwise \end{cases} \tag{5.2.8}$$

where l_e is the length of $\mathcal{S}_e$ (see Fig. 6.b). Substitution of eq.(5.2.8) into eq.(5.2.7), considering eq.(5.1.8), leads to:

$$\int_{\mathcal{S}_e} \boldsymbol{\sigma}^h \cdot \boldsymbol{\mathcal{N}} \, d\Gamma - \frac{l_e}{\Omega_e} \int_{\Omega_e \backslash \mathcal{S}_e} \boldsymbol{\sigma}^h \cdot \boldsymbol{\mathcal{N}} \, d\Omega_e = 0 \tag{5.2.9}$$

which can be rewritten as:

$$\underbrace{\frac{1}{l_e} \int_{\mathcal{S}_e} \boldsymbol{\sigma}^h \cdot \boldsymbol{\mathcal{N}} \, d\Gamma}_{average \; on \; \mathcal{S}_e} = \underbrace{\frac{1}{\Omega_e} \int_{\Omega_e \backslash \mathcal{S}_e} \boldsymbol{\sigma}^h \cdot \boldsymbol{\mathcal{N}} \, d\Omega_e}_{average \; on \; \Omega_e \backslash \mathcal{S}_e} \tag{5.2.10}$$

Inspection of eq.(5.2.10) shows that they enforce, in average, eq.(5.2.5). Therefore *eq.(5.2.7) enforces, with mesh refinement, the traction vector continuity condition.*

In summary, the discretized set of equations:

$$\begin{aligned} \int_{\Omega} \mathbf{B}^T : \boldsymbol{\sigma}^h \, d\Omega &= \mathbf{f}_{ext} \\ \int_{\Omega_e} \mathbf{G}_e^{*T} \cdot \boldsymbol{\sigma}^h \, d\Omega_e &= 0 \qquad e = 1...n_{el} \end{aligned} \tag{5.2.11}$$

where $\boldsymbol{\sigma}^h(\boldsymbol{\epsilon}^h)$ comes from the chosen nonlinear constitutive equation with distributional strain softening, and $\boldsymbol{\epsilon}^h$ is given by eqs.(5.1.9) to (5.1.11) in terms of the nodal displacement vector $\mathbf{a}$ and the elemental jumps $\boldsymbol{\alpha}_e$, provide a sufficient set of equations for the determination of the set of unknowns $\mathbf{a}, \boldsymbol{\alpha}_e$. It is expected that, at a given time of the analysis, the jump $\boldsymbol{\alpha}_e$ is different from zero only in those elements belonging to Ω_h, thus defining the path of elements crossed by $\mathcal{S}$ at this time (see. Fig. 6a).

For the considered case of linear triangular elements the strain field is piecewise constant in both $\Omega_e \backslash \mathcal{S}_e$ and $\mathcal{S}_e$ and, consequently, so are the corresponding stress fields coming from the constitutive equation. Since the measures of $\mathcal{S}_e$ and $\Omega_e \backslash \mathcal{S}_e$ are l_e and $\bar{\Omega}_e$, respectively, eq.(5.2.10) can we rewritten as:

$$\boldsymbol{\sigma}^h_{\mathcal{S}_e} \cdot \boldsymbol{\mathcal{N}} = \boldsymbol{\sigma}^h_{\Omega_e \backslash \mathcal{S}_e} \cdot \boldsymbol{\mathcal{N}} \tag{5.2.12}$$

and, thus, eq.(5.2.5) is piecewise fulfilled on the elements belonging to Ω_h.

REMARK (5.2.2)
Eq.(5.2.12) is obtained independently of the value of l_e considered in eqs.(5.2.9), whenever the same value for l_e is taken in the factor $\frac{l_e}{\bar{\Omega}_e}$ and as the length (measure) of $\mathcal{S}_e$. From this, and from the considerations done in remark 5.2.1, we conclude that l_e plays no specific role in the formulation and that any value for l_e can be considered.

REMARK (5.2.3)
Observe that the matrix $\mathbf{G}_e^*$ appearing in eqs.(5.2.8) and (5.2.11)) fulfills the following condition:

$$\int_{\Omega_e} \mathbf{G}_e^* \, d\Omega = 0 \tag{5.2.13}$$

as can be easily checked taking into account eq.(5.1.8). It is also possible to check, from eqs.(5.1.10) to (5.1.12), that the spaces generated by the regular strains $\hat{\boldsymbol{\epsilon}}^h$ and the enhanced strains $\tilde{\boldsymbol{\epsilon}}^h$, denoted by $\hat{\boldsymbol{\mathcal{V}}}^h$ and $\tilde{\boldsymbol{\mathcal{V}}}^h$ respectively, are such that:

$$\hat{\boldsymbol{\mathcal{V}}}^h \cap \tilde{\boldsymbol{\mathcal{V}}}^h = \emptyset \tag{5.2.14}$$

Conditions (5.2.13) and (5.2.14) are sufficient to guarantee the consistency and stability requirements for the proposed assumed strain approximation[17].

The tangent matrix corresponding to the discretized set of equations (5.2.11) can be easily derived by resorting to the constitutive tangent operator $\boldsymbol{\mathcal{C}}^{tg}$ defined through:

$$\dot{\boldsymbol{\sigma}}^h = \boldsymbol{\mathcal{C}}^{tg} : \dot{\boldsymbol{\epsilon}}^h \tag{5.2.15}$$

In view of eqs.(5.1.9) to (5.1.11), standard arguments lead to the elemental contribution to the tangent matrix as:

$$\mathbf{K}_e = \int_{\Omega_e} \begin{bmatrix} \mathbf{B}_e^T \cdot \boldsymbol{\mathcal{C}}^{tg} \cdot \mathbf{B}_e & \mathbf{B}_e^T \cdot \boldsymbol{\mathcal{C}}^{tg} \cdot \mathbf{G}_e \\ \mathbf{G}_e^{*T} \cdot \boldsymbol{\mathcal{C}}^{tg} \cdot \mathbf{B}_e & \mathbf{G}_e^{*T} \cdot \boldsymbol{\mathcal{C}}^{tg} \cdot \mathbf{G}_e^* \end{bmatrix} d\Omega_e \qquad (5.2.16)$$

where $\mathbf{B}_e$ stands for the deformation matrix restricted to the element e. Observe, from eqs.(5.1.12) and (5.2.8) that, except for very particular cases‡ $\mathbf{G}_e \neq \mathbf{G}_e^*$. Therefore, even for the frequent case of symmetric $\boldsymbol{\mathcal{C}}^{tg}$, the present formulation is unsymmetric. This could be expected since the traction vector continuity condition (5.2.5) is not imposed via a variational framework.

REMARK (5.2.4)
The preceding formulation ruled by the discretized system of equations (5.2.11) enjoys all the advantages of the A.E.S methods, in particular the ones related to the easiness of implementation. For practical purposes the implementation in a standard finite element code requires only the consideration, for each element, of an additional (internal) node with two degrees of freedom (the displacement jumps), which does not contributes to the external forces vector $\mathbf{f}_{ext}$ (see eq. 5.2.11). Then, for strain computation purposes the standard deformation matrix, $\mathbf{B}_e$ has to be extended to one fourth node considering the matrix $\mathbf{G}_e$ (see eqs.(5.1.9) to (5.1.12)). For the purposes of computation of the residual forces vector, $\mathbf{B}_e$ has to be extended to the fourth node considering the matrix $\mathbf{G}_e^*$ of eq.(5.2.8). Moreover, computational savings can be obtained by condensing, at elemental level, the contributions of the fourth node to the tangent matrix and to the residual forces vector[17].

5.3. Regularization via delta-sequences. Regularized softening parameter. Integration rule.

In the present approach we have to get round the obstacle of dealing with delta-functions, as the ones appearing in eqs.(2.6), (5.1.12) and (5.2.8). In order to circumvent the difficulties inherent to perform computations involving Dirac's delta-functions in standard computers, we proceed to regularize the formulation by defining a delta-sequence, by means of a *regularization parameter* k, which converges to a delta-function when k tends to zero (in practice k can be as small as permitted by the machine precision). Therefore, the delta function δ_{S_e} is replaced by a regularized delta-sequence $\delta_{S_e}^k$.

The simplest way to construct $\delta_{S_e}^k$ is by considering a finite band Ω_e^k (from now on termed the *elemental discontinuity band*) of width k (see Fig. 8.a) around the elemental discontinuity line $\mathcal{S}_e$, and defining (see Fig 8b):

$$\delta_{S_e}^k(\mathbf{x}) = \begin{cases} \dfrac{1}{k} & \forall\, \mathbf{x} \in \Omega_e^k \\ 0 & otherwise \end{cases} \qquad (5.3.1)$$

‡ It can be shown that if $\mathcal{S}_e$ is parallel to one side of the triangle, then $\mathbf{G}_e = \mathbf{G}_e^*$ and the formulation becomes symmetric.

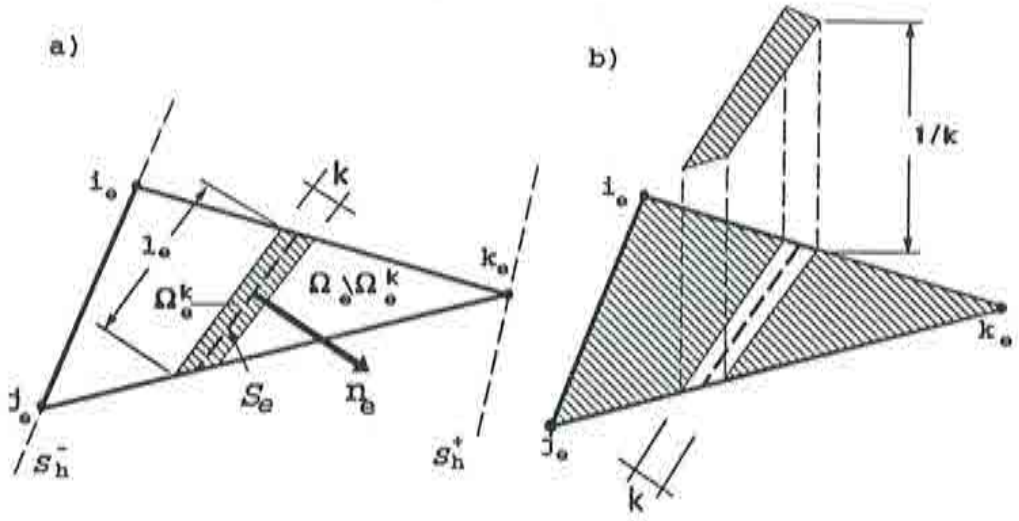

Figure 8. *Regularized delta-sequence.*

In view of eq.(5.3.1) the softening parameter $\mathcal{H}$ of eq.(2.6) can be now replaced in the constitutive equation by the *regularized softening parameter* $\mathcal{H}^k$ defined as:

$$\mathcal{H}^k(\mathbf{x}) = \begin{cases} k\bar{\mathcal{H}} & \forall\, \mathbf{x} \in \Omega_\epsilon^k \\ \\ \infty & \textit{otherwise (elastic behaviour)} \end{cases} \tag{5.3.2}$$

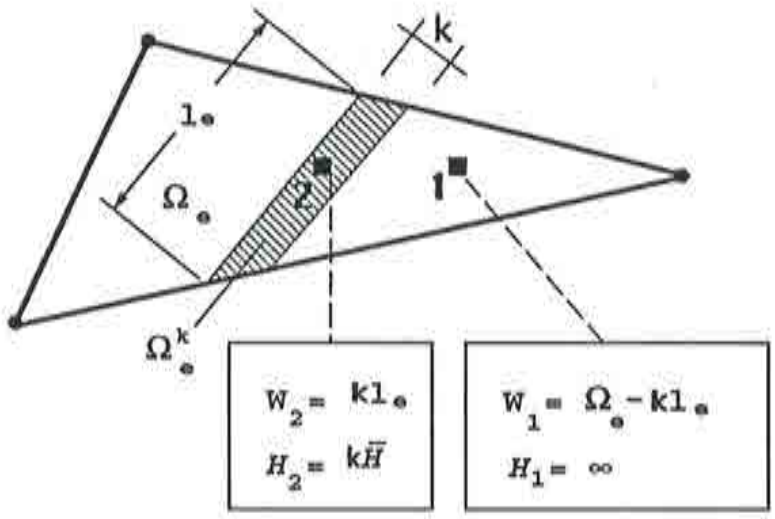

Figure 9. *Numerical integration rule and regularized hardening-softening parameter.*

REMARK (5.3.1)
To some extent the regularization parameter k plays, in the present formulation, the role of the so called characteristic length[8] *in some continuum models for capturing localization phenomena, which has a direct dependence on the mesh size. In both cases this parameter affects the slope of the softening branch of the constitutive equation but here k does not depends on the mesh size at all. Eq.*$(5.3.2)_1$ *shows that, when k tends to zero, the limit case of perfect plasticity or perfect damage* ($\mathcal{H} = 0$) *is approached.*

Consideration of the regularized elemental discontinuity band Ω_e^k suggests an specific numerical integration rule for the described element. Inspection of the resulting formulation in sections 5.1 and 5.2, in view of eqs.(5.3.1) and (5.3.2), reveals that the strains (and consequently the stresses) are piecewise constant in both the domains Ω_e^k and $\Omega_e \backslash \Omega_e^k$ (see Fig. 9). Thus, after examining the set of equations to solve (5.2.11) we conclude that only one integration point is needed in each of those domains, whose weight is the corresponding area according to the following table:

Point	**Domain**	**Weight**
1	$\Omega_e \backslash \Omega_e^k$	$meas[\Omega_e] - kl_e$
2	Ω_e^k	kl_e

where $meas[\Omega_e]$ stands for the area of Ω_e. No specific location for the integration points, at the corresponding domain, needs to be specified.

6. ADDITIONAL COMPUTATIONAL ASPECTS: THE DISCONTINUITY PATH

Along section 5 the location of the discontinuity line $\mathcal{S}$ over the body Ω has been assumed known. If so, the rest of the formulation can be precisely defined as described there. Therefore, in this section the attention is focused on the determination of the following aspects:

I) If a given element e is crossed by $\mathcal{S}$ and, thus, belongs to Ω_h (see Fig. 6.a).

II) If so, what sides of the element are crossed by $\mathcal{S}$ and, then, which is the *solitary node* k_e (see Fig. 6.b). From this, the shape function N_{k_e} can be determined in eq.(5.1.12).

III) The normal $\mathbf{n}_e$ (see Fig. 6.b). Then, $\mathbf{G}_e$ (eq.(5.1.12) and $\mathbf{G}_e^*$ (eqs.(5.2.6) and (5.2.8)) can be completely determined.

Concerning to these aspects in the proposed methodology distinction is made between:

- *Active elements*: Those elements which, at a certain considered time t, capture the discontinuity. In the context of a quasistatic analysis the active elements determine the domain Ω_h, surrounding the discontinuity line S, which advances along time, as long as the external actions are increased (see Fig. 6a). Those elements are characterized by both having a non-zero jump ($\alpha_e \neq 0$) and a softening behaviour at the integration point 2. Once signaled by the algorithm described in the next section they remain active for the rest of the analysis.

- *Unactive elements*: those elements that, at a given time, are not active.

For unactive elements, determination of k_e and $\mathbf{n}_e$ is not relevant. Both are arbitrarily stated at the beginning of the analysis with the only requirement that eq.(5.2.13) is satisfied. These values remain unchanged unless the element becomes active.

6.1. Determination of the discontinuity path across the element: a tracking algorithm.

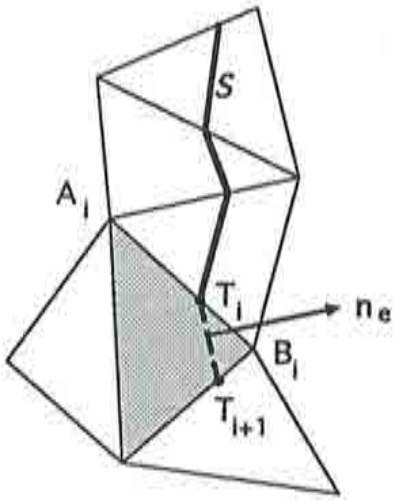

Figure 10. *Discontinuity path tracing algorithm.*

Concerning to the aspects I) and II) described above, a recursive *discontinuity path tracing algorithm*, based on the identification of the *discontinuity front*, that is, the end T_i of the current discontinuity line at time t_i, (see Fig. 10) has been devised as follows:

1) At time t_i the position of point T_i, assumed to be placed on an element side, is known and identified by the relative distance of T_i to the corresponding nodes A_i and B_i (see Fig. 10).

2) During the iterative resolution at time step t_{i+1}, the integration point **2** of the neighbor unactive element (sharing the point T_i with the current *front* element) is continuously reexamined. As soon as the constitutive behaviour at this point becomes inelastic the normal $\mathbf{n}_e$ is computed as indicated in section 6.2 below. From the current *discontinuity front* T_i and the value of $\mathbf{n}_e$, very simple geometric computations allow to determine the next *discontinuity front* T_{i+1} and the corresponding *solitary node* k_e ($k_e = B_i$ in Fig. 10). In subsequent iterations the discontinuity line is allowed to advance from T_{i+1} to reach neighbor elements.

3) Once convergence is achieved at time t_{i+1} the discontinuity path is updated: the new affected elements are declared active and the corresponding values for the normal and the *solitary node* are kept fixed for next time steps.

6.2. Determination of the normal

In Part I of this work[12] (sections 4.4 and 5.4) a procedure for the determination of the normal to the discontinuity line has been presented. In particular, for 2D cases closed form formulas, for the determination of the inclination angle θ with respect to an orthonormal basis, have been given. Those formulas allow the computation of θ in terms of the *bounded part of the strain* in S at the initiation time ‡. In other words: in terms of the strain at the integration point **2** defined in section 5.3 (see also Fig. 9). For instance, considering the isotropic damage model described in Part I and denoting by $\boldsymbol{\epsilon}_2^0 = \{\epsilon_{xx}^0, \epsilon_{yy}^0, 2\epsilon_{xy}^0\}_2$ the strain vector, in a cartesian coordinate system (x, y), where superscript $(\cdot)^0$ refers to the initiation time t_0 and subscript $(\cdot)_2$ refers to the integration point **2**, the inclination angle reads:

$$\theta_e \;=\; atan\left[\; \frac{\epsilon_{xy}^0 \;\pm\; \sqrt{(\epsilon_{xy}^0)^2 \;-\; \epsilon_{xx}^0\;\epsilon_{yy}^0}}{\epsilon_{xx}^0} \;\right]_2 \qquad (6.2.1$$

As soon as the element is detected as candidate to be the *front element* by the algorithm described in section 6.1, the corresponding inclination angle θ_e is computed and, then, the normal $\mathbf{n}_e = \{n_x, n_y\}$ as:

$$n_x \;=\; cos\;\theta_e \qquad\qquad n_y \;=\; sin\;\theta_e \qquad (6.2.2)$$

REMARK (6.2.1)
Eq.(6.2.1) provides, in general, two different values for θ_e and, thus, two different possible inclinations of the discontinuity line at the element e. Therefore, two different incompatible modes per element would have to be considered in section 5. In fact, only for the very particular case of having two discontinuity lines crossing the same element, both modes would be simultaneously active. For the sake of simplicity, in the examples presented below only the mode corresponding to the largest value of θ_e (sign + in eq.(6.2.1)) has been considered.

‡ for a given point, the time of the analysis at which the discontinuity initiates.

7. NUMERICAL EXPERIMENTS

To illustrate the preceding methodology some numerical simulations, considering different constitutive models and several types of strong discontinuities, are presented in next sections.

7.1. Uniaxial tension test using a continuum damage model.

In Fig. 11 the considered geometry, loading and boundary conditions are depicted.

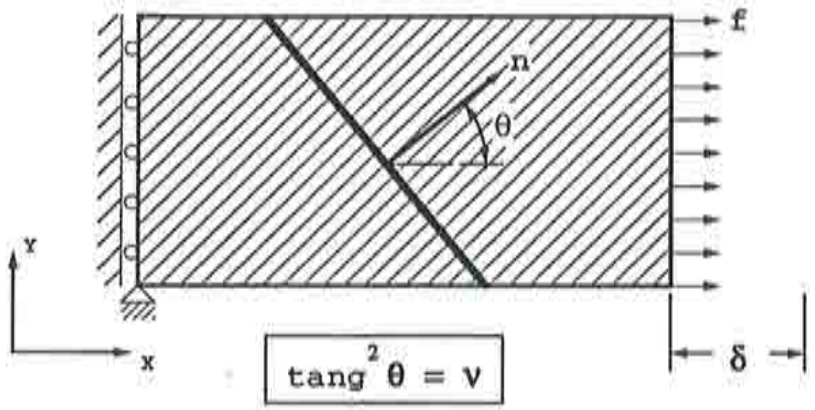

Figure 11. *Uniaxial tension test using a continuum damage model: definition of the problem.*

In a first step the continuum damage model described in section 4 of Part I is considered and the problem is analyzed under plain stress conditions. For this case the analytical solution can be obtained: perturbation of the peak stress σ_u at a certain material point leads to the formation of a strong discontinuity, along a straight line passing through the perturbed point. The inclination angle θ of the discontinuity line with respect to the x axis is given by (see Part I[12], eq.(III.5)):

$$\theta = \sqrt{\nu} \tag{7.1.1}$$

where ν stands for the Poisson's ratio.

The analytical solution also exhibits an uniaxial and smooth stress field given by: $\sigma_x = \sigma, \quad \sigma_y = 0, \quad \tau_{xy} = 0$. In Fig. 12 numerical simulations for $\nu = 0.4$ are presented. Thus, from eq.(7.1.1), a value of $\theta = 32.31^0$ is expected for the inclination angle. In a first stage a finite element mesh with a structured band of elements defined by two parallel lines with this inclination is considered (see Fig. 12.1). The peak stress of the upper element of this band is slightly reduced (1%) in order to trigger the discontinuity. Fig. 12.2 shows the deformed mesh (amplified 100 times) ‡ exhibiting an almost rigid body motion of the frontal

‡ For all the results presented here, postprocessing is based on the nodal values corresponding to the regular displacement field $\hat{\mathbf{u}}^h(\mathbf{x}, t)$ (see eq.(5.1.1)). Thus, *the enriching incompatible modes are not considered for postprocessing purposes.*

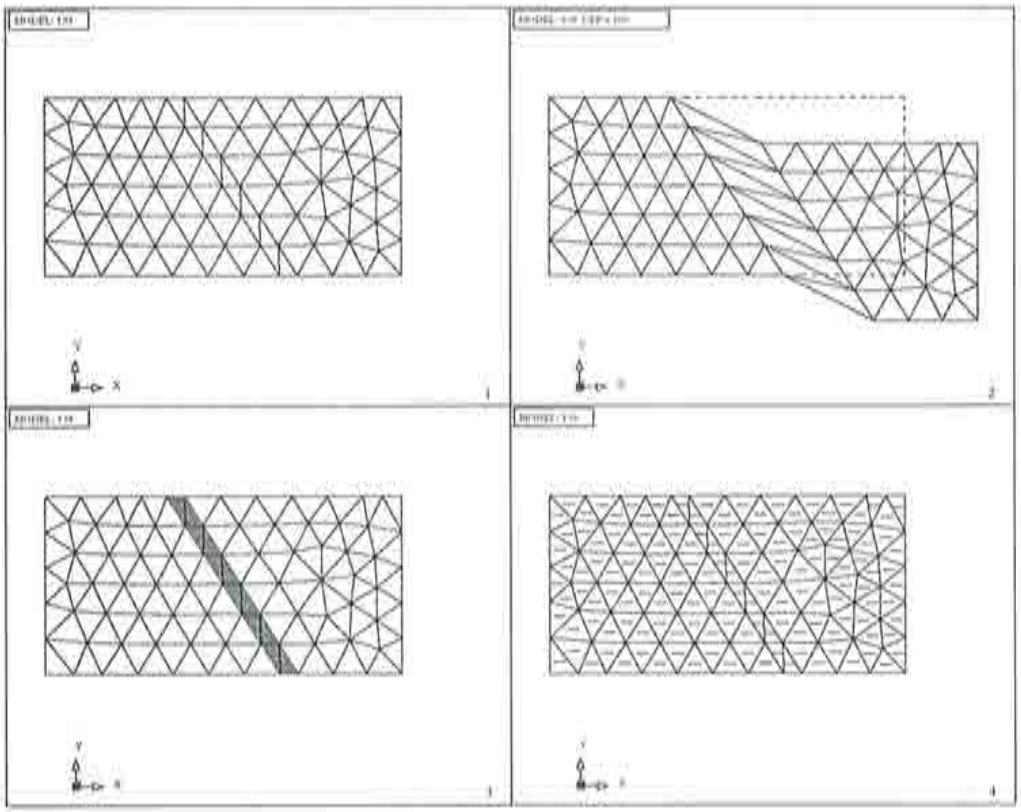

Figure 12. *Uniaxial tension test using a continuum damage model: results with the structured mesh.*

part of the specimen which corresponds to a mixed (Mode I-Mode II) mode of fracture. Observe that the jump is perfectly captured by the inclined band as is stated in Fig. 12.3 by the contours of the total displacement field, which uniformly group inside this band. Fig. 12.4 shows the principal stress field which is uniaxial and perfectly smooth.

Results in Fig.13 are force-displacement ($f - \delta$ in Fig. 11) curves at the right-hand side end of the specimen for different values of the width of the structured band (h=1.0 and h=0.01) and the regularization parameter (k=1.0e-03 and k=1.0e-09). In all the cases the differences are indistinguishable in the plots, so *complete insensitivity with respect to the size of the finite elements capturing the jump* (mesh size objectivity) *and with respect to the value of the regularization parameter*, assumed to be small enough with respect to the size of the element, *is shown*. In a second stage the same problem is analyzed with an *unstructured* finite element mesh (see Fig. 14.1). Again the computed deformed mesh (Fig. 14.2), contours of the total displacement (Fig. 14.3) and the principal stress field (Fig. 14.4) are presented. The results are *exactly the same than in the previous case*. The only difference is that, now, the discontinuity is captured by a band of elements which zig-zagges through the mesh which contains the discontinuity line whose inclination angle is, as expected, $\theta = 32.31^0$.

In Fig. 15 the force-displacement curves at the end of the specimen are compared for both the structured and the unstructured meshes. Both curves

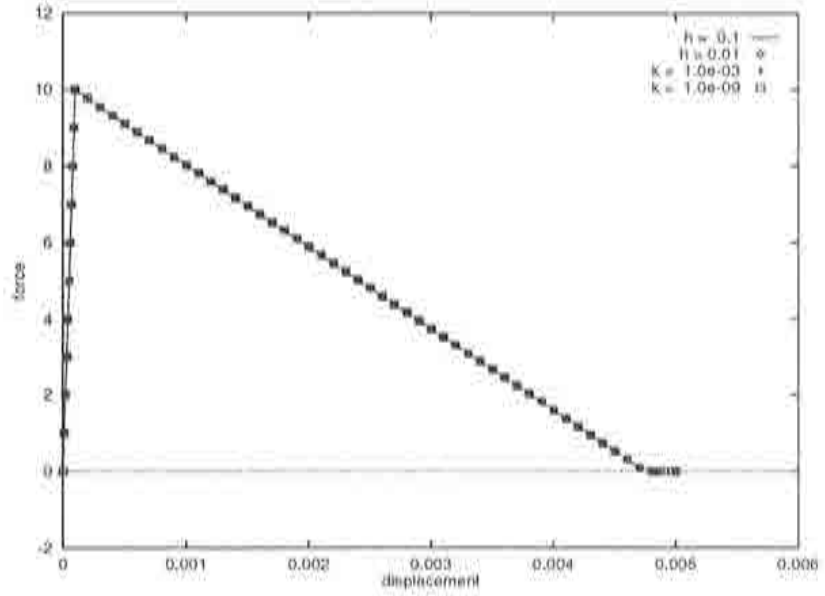

Figure 13. *Uniaxial tension test using a continuum damage model: Sensitivity analysis with respect to the finite element size, h, and the regularization parameter, k.*

are indistinguishable in the plot, thus, *complete insensitivity with respect to the mesh alignment is exhibited.*

7.2. Simulation of a slip line using a J2 plasticity model.

Next analysis considers a J2 plasticity model under plane strain conditions in a specimen uniaxially compressed as shown in Fig. 16.1. Theoretical results (see Part I[12], section 5 and appendix II and III) predict the formation of a slip line inclined 45^0 with respect to the vertical axis (the direction of the maximum principal stress). The corresponding numerical results, for the unstructured finite element mesh shown in Fig. 16.2, are presented in Figs. 16.3 and 16.4. After a small perturbation of the yield stress in a certain element of the top of the mesh, the deformed mesh (amplified 100 times) shown in Fig. 16.3 is obtained. The discontinuity is captured by the band of elements highlighted by means of the total displacement contours in Fig. 16.4, which contains the slip line (not shown in the plot) exactly inclined 45^0.

7.3. Mode I fracture simulation

This test corresponds to the mode I fracture simulation of a notched specimen using a continuum damage model with nonsymmetric tension-compresion behaviour and exponential softening (see Part I[12], Appendix I). In Fig. 17 the geometry and the considered finite element mesh are depicted. The mesh is completely unstructured, unsymmetric and slightly refined in the zone where the discontinuity is expected to appear.

Fig. 18 shows the progression of the discontinuity along increasing times of the analysis. The discontinuity path is identified by the contours of equal horizontal displacement which group along the elements capturing the

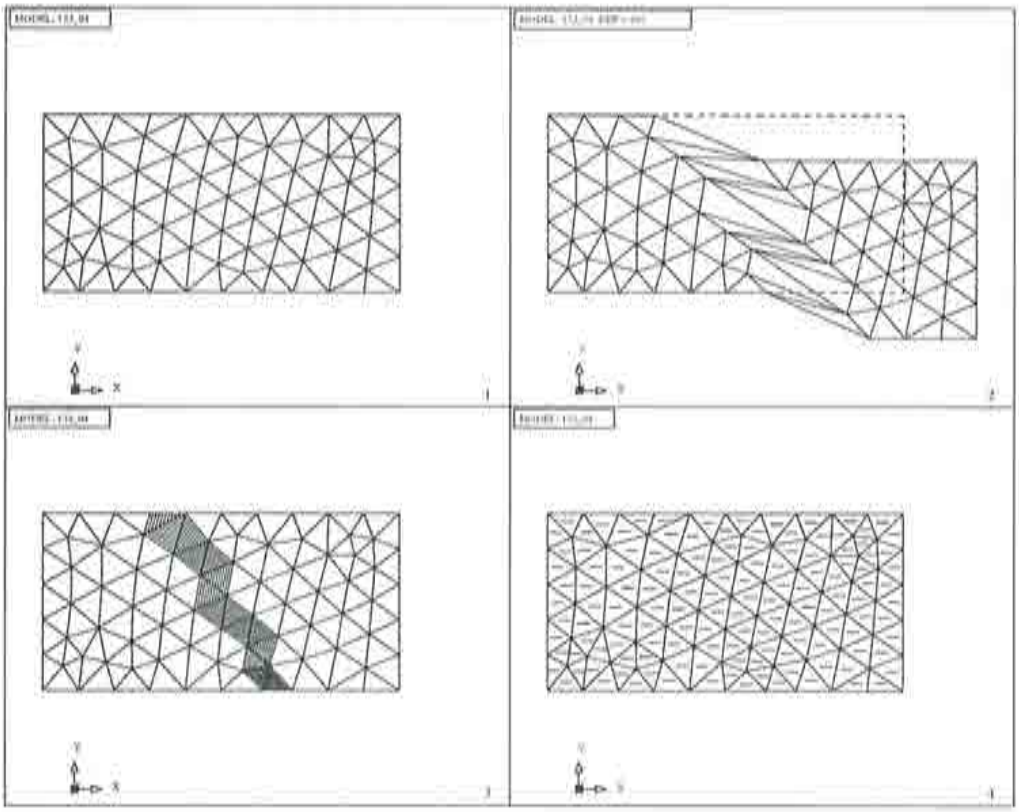

Figure 14. *Uniaxial tension test using a continuum damage model; results with the unstructured mesh.*

discontinuity (in black color in the figure). Though this path of elements zig-zagges vertically along the mesh, the captured discontinuity line (not plotted) is, as expected, a *vertical straight line* starting at the notch tip and crossing all the elements of the band.

Fig. 19.a shows the deformed mesh (amplified 300 times) at the end of the analysis where the localization of the regular strain field along the band of elements capturing the discontinuity can be observed. Fig. 19.b corresponds to the projection of the total displacement on the third dimension showing the linear variation of the jump along the discontinuity line.

8. CONCLUSIONS

In this work a possible approach to the numerical simulation of strong discontinuities in solids has been presented. Making use of the results provided by the strong discontinuity analysis of standard constitutive equations[9,11,12,18,19] a finite element methodology of simulation has been derived. Taking as underlying element the simple 3-noded linear triangle the addition of a suitable incompatible mode and one integration point allows for the appropriate capture of the displacement jumps as shown in the numerical simulations. In opinion of the author several advantages of the proposed methodology, with respect to some

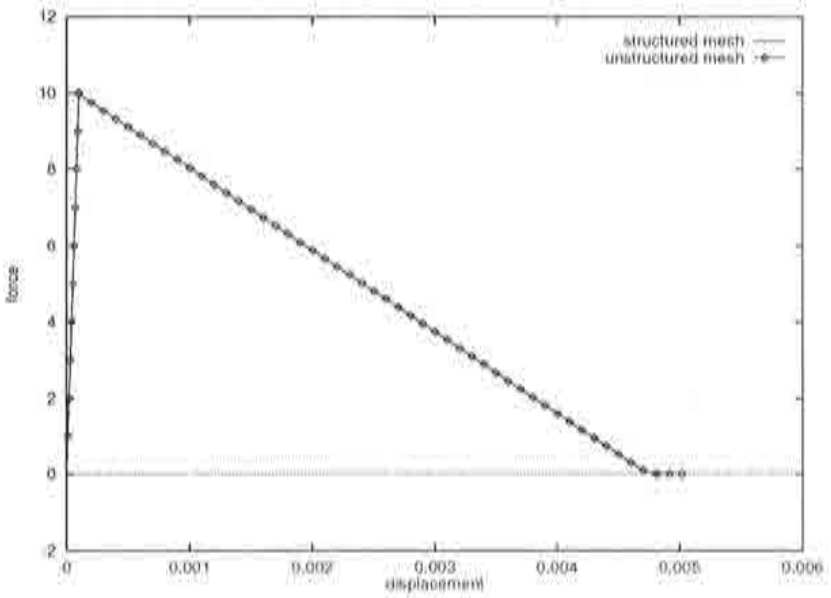

Figure 15. *Uniaxial tension test using a continuum damage model: force-displacement curves for the structured and the unstructured meshes.*

existing alternatives, should be highlighted:

- Standard (local, stress-strain) constitutive equations can be considered without having to resort to specific (rate-dependent[7], non local[15], gradient-dependent[2], Cosserat-type[2] etc.) constitutive equations. The only requirement is the inclusion in the constitutive equation, after the elastic regime, of a *softening branch* responsible for the formation of the strong discontinuity and for the local dissipation along the discontinuity path, which, in the most general case, could be preceded by a non-linear *hardening* branch responsible for the non-linear behavior outside the discontinuity path and for the volume dissipation. Therefore, the same constitutive equation would model the standard non linear behaviour appearing before the formation of the strong discontinuity and the strong discontinuity itself, thus providing a continuous transition between both regimes. In principle it does not appear any restriction on the type of constitutive equation to be considered. Therefore those families of constitutive equations which have shown suitable for modelling the non-linear (hardening) behaviour of the different types of solids (concrete, metals, soils etc.) could be considered, just by the addition of a softening branch, for the simulation of strong discontinuities in the same type of solids.

- Numerical difficulties, typical of continuum approaches to strong discontinuities, as finite element size and mesh alignment dependencies[16], can be removed. If the stress field can be exactly captured by the underlying element (as is the case of the uniaxial tension tests shown above where the triangular element is able to capture exactly the constant stress field solution of the problem) the provided solution of the strong discontinuity problem *is*

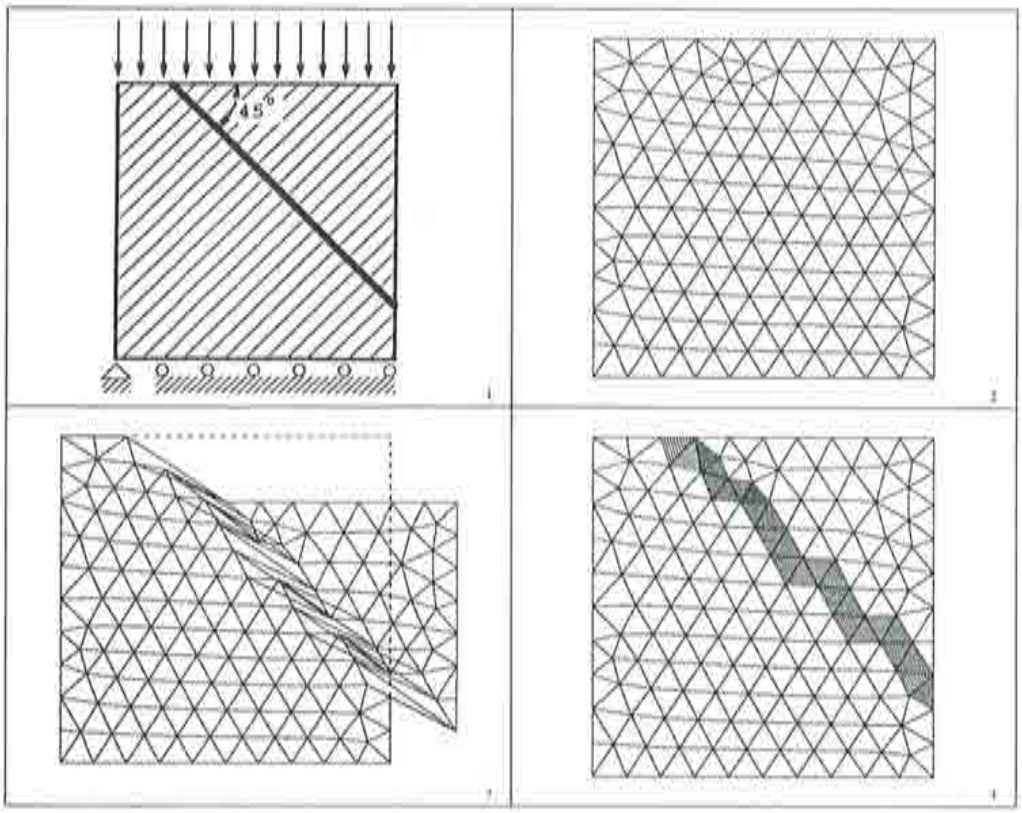

Figure 16. *Simulation of an slip-line using a J2 plasticity model: 1) definition of the problem, 2,3,4) numerical results.*

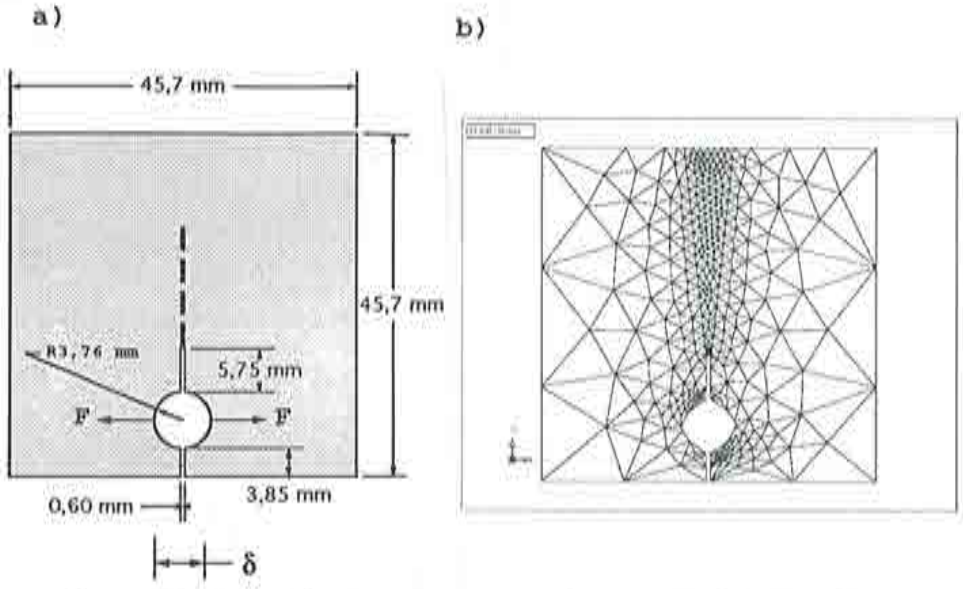

Figure 17. *Mode I fracture simulation: a) geometric definition b) finite element mesh.*

exact and completely independent of the shape and size of the finite element

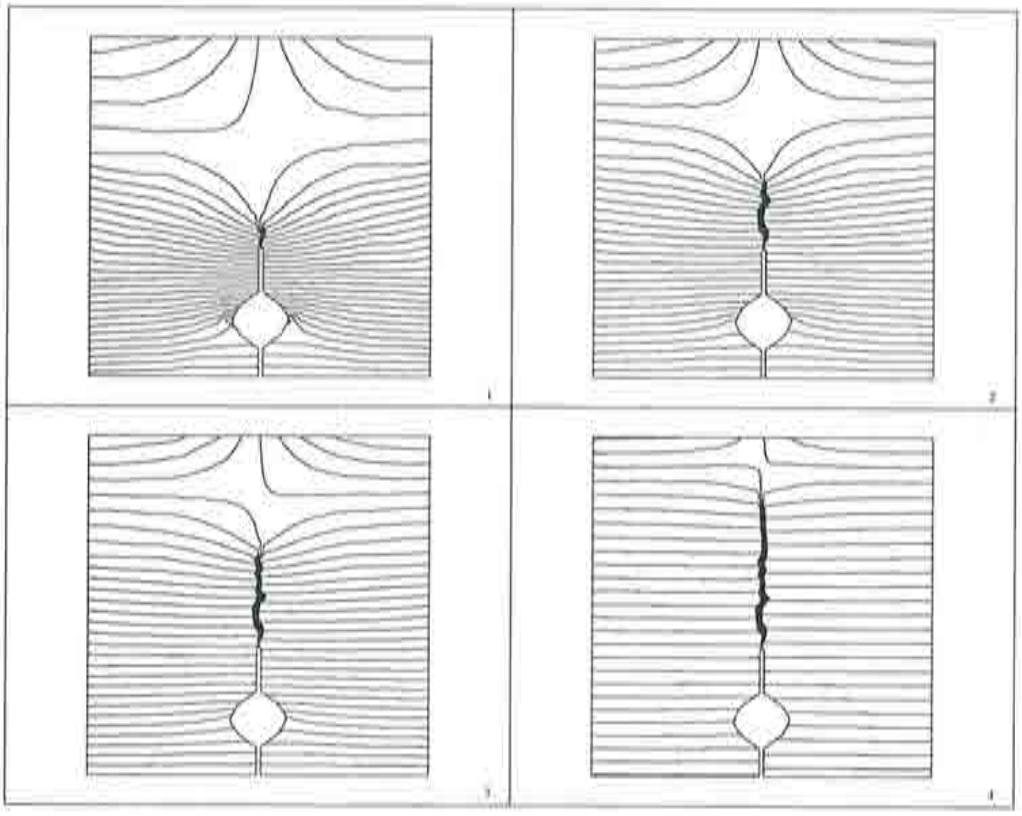

Figure 18. *Mode I fracture simulation: from 1) to 4) progression of the discontinuity path for increasing times of the analysis.*

mesh. In other words: mesh refinement could be envisaged not as an specific way to capture the discontinuity [14,22] but, as in standard problems, a tool to improve the overall approximation of the numerical solution.

- As said above (section 5) the presented finite element approach, based on the use of regularized delta-functions and the *weak* imposition of the traction vector continuity condition, can be inscribed in the family of the assumed enhanced strain methods (A.E.S). Although several different alternatives could be imagined, resorting to A.E.S method has the crucial advantage of the easiness of implementation in any existing non-linear finite element code. In fact, the structure of the code remains the same and only an additional internal node has to be considered for each element. In consequence, the code has only to be modified at the low (elemental) level and the rest of its structure and facilities remain unchanged.

- Theoretically, no special difficulties are envisaged to extend the presented formulation to other type of finite elements (higher order triangles and quadrilaterals) and other non-linear constitutive equations. Even the extension to the general 3D case seems to follow naturally. Anyway, this would have to be proved by the corresponding implementations.

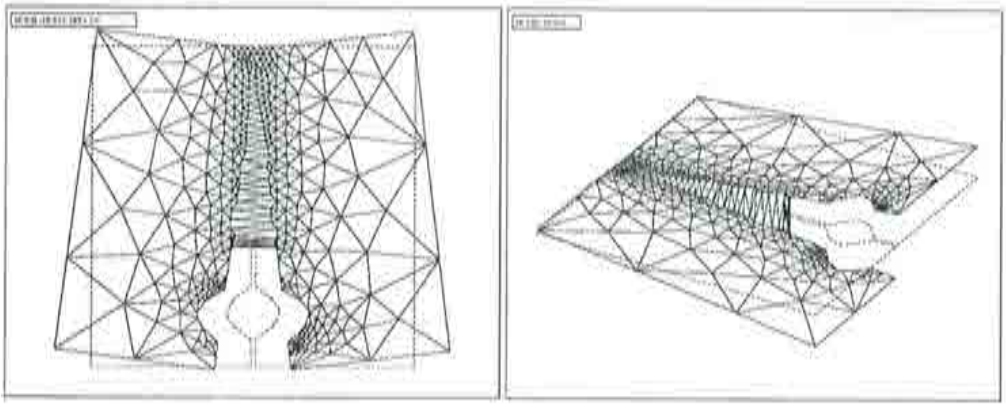

Figure 19. *Mode I fracture simulation: a) deformed mesh (amplified 300 times) and b) 3D representation of the jump (the total displacement values are plotted along the third dimension).*

On the other hand, from the experience obtained in the numerical simulations carried out in this work, some *weak points* of the approach emerge:

- Although the tracking algorithm presented in section 6.1 has shown able to provide the right discontinuity path in the simulations, it is a *global* algorithm which requires, for each element, information from the neighbor elements. This fact could be a drawback for finite element codes based on elemental data-basis. In this sense, a *local* algorithm would be preferable.

- Determination of the right discontinuity path has shown to play a crucial role for the appropriate solution of the strong discontinuity problem and for the convergence of the non-linear solution scheme. This determination lies crucially on the acurate computation of the normal to the discontinuity path which, in turn, depends on the goodness of the captured regular strain field at the initiation time (see Part I[12], eqs.(4.4.8) and (5.4.3)). For low order elements, as the linear triangle used in the examples presented above, this fact could, by itself, increase very much the required number of elements in the mesh.

- In connection with the preceding considerations, convergence of the standard Newton-Raphson schemes for the solution of the non-linear problem was found to require very small time steps in the initial stages of the analysis (even if consistent tangent operators were used). Once most part of the discontinuity path was traced the rest of the analysis could be conducted under much larger time steps. In this sense appropriated algorithms to increase the robustness of the non-linear analysis seem to be needed.

9. ACKNOWLEDGEMENTS

The author wishes to express his gratitude, admiration and remembrance to the figure of Professor Juan C. Simo, from the Stanford University (U.S.A). Large part of this work was developed in close collaboration with him during the last years of his life.

REFERENCES

[1] BELYTSCHKO T., FISH J. and ENGELMANN B.E. A finite element with embedded localization zones. Comp. Meth. Appl. Mech. Engng., 70, 59-89, 1988

[2] De BORST R., MUHLHAUS H.B., PAMIN J., and SLUYS L.J. Computational Modelling of Localisation of Deformation. In: D.R.J. Owen et. al., editors, *Proc. of the Third Conference on Computational Plasticity: Fundamentals and Applications*, 483-508, Pineridge Press, Swansea, 1992

[3] DVORKIN E.N., CUITIÑO A.M and GIOIA G. Finite elements with displacement interpolated embedded localization lines insensitive to mesh size and distortions. Int. Journ. Num. Meth. Engng., 30, 541-564, 1990

[4] LARSSON. R. RUNESSON K. and OTTOSEN N.S. Discontinuous displacement approximation for capturing plastic localization. Int. Journ. Num. Meth. Engng., 36, 2087-2105, 1993

[5] LOFTI H.R. and SHING P.B. Analysis of concrete fracture with an embedded crack approach. In: H. Mang et. al., editors, *Proc. EURO-C 1994 Computer Modelling of concrete structures*, 343-352, Pineridge Press, Swansea, 1994

[6] MAMIYA E. and SIMO J.C. Numerical analysis of equilibrium shocks and phase transitions in non linear elasticity. Journal of Elasticity, 1994

[7] NEEDLEMAN A. Material Rate Dependence and Mesh Sensitivity in Localization Problems. Comp. Meth. Appl. Mech. Engng., 67, 69-86, 1988

[8] OLIVER J. A consistent characteristic length for smeared cracking models. Int. Journ. Num. Meth. Engng., 28, 461-474, 1989

[9] OLIVER J. Continuum modelling of strong discontinuities in solid mechanics. In: D.R.J. Owen et. al., editors, *Proc. COMPLAS IV, Fourth international conference on computational plasticity*, 455-479, Pineridge Press, Swansea, 1995

[10] OLIVER J., CERVERA M., OLLER S. and LUBLINER J. Isotropic damage models and smeared crack analysis of concrete. In: N. Bicanic et. al., editors, *Proc. SCI-C Computer Aided Analysis and Design of Concrete Structures*, 945-957, Pineridge Press, Swansea, 1990

[11] OLIVER J. and SIMO J.C. Modelling strong discontinuities by means of strain softening constitutive equations. In: H. Mang et. al., editors, *Proc. EURO-C 1994 Computer Modelling of concrete structures*, 363-372, Pineridge Press, Swansea, 1994

[12] OLIVER J. Modelling strong discontinuities in solid mechanics via strain softening constitutive equations. Part I: Fundamentals.

[13] ORTIZ M., LEROY Y. and NEEDLEMAN A. A finite element method for localized failure analysis. Comp. Meth. Appl. Mech. and Eng., 61, p.p 189-214, 1987

[14] PERIC D., YU J.. and OWEN D.R.J. On error estimates and adaptivity in elastoplastic solids: Applications to the numerical simuulation of strain localization in classical and Cosserat continua. Int. J. Num. Meth in Engng., Vol 37, p.p 1351-1379, 1994

[15] PIJAUDIER CABOT G. and BAZANT Z.P. Nonlocal Damage Theory. Jour. Engng. Mech., A.S.C.E., 113, 1512-1533, 1987

[16] ROOTS J.G. Computational modeling of concrete fracture, Ph. D. Thesis, Delft University of Technology, Delft, Netherlands, 1988.

[17] SIMO, J.C. and RIFAI S. A class of mixed assumed strain methods and the method of incompatible modes. Int. Journ. Num. Meth. Engng., 29, 1595-1638, 1990

[18] SIMO J.C., OLIVER J. and ARMERO F. An analysis of strong discontinuities induced by strain-softening in rate-independent inelastic solids. Computational Mechanics, 12, 277-296, 1993

[19] SIMO J.C. and OLIVER J. A new approach to the analysis and simulation of strong discontinuities. In: Z.P. Bazant et. al., editors, *Fracture and Damage in Quasibrittle Structures*, 25-39, E & FN Spon, 1994

[20] STEINMANN P., WILLAM K. Performance of enhanced finite element formulations in localized failure computations. Comp. Meth. Appl. Mech. and Eng., 90, p.p 845-867, 1991

[21] ZIENKIEWICZ O.C. and TAYLOR R.L. *The Finite Element Method*, McGraw-Hill, London, 1989

[22] ZIENKIEWICZ O.C., HUANG M. and PASTOR M. Localization problems in plasticity using finite elements with adaptive remeshing. Int. Journ. Num. Meth. Engng., 19, 127-148, 1995